OUKA
The University of Osaka
Institutional Knowledge Archive

Title	Liver Sinusoidal Endothelial Cells Promote Metabolic Dysfunction-associated Steatohepatitis Progression via Interleukin-1R1-mediated Chemokine Production Induced by Macrophage-derived Interleukin-1β
Author(s)	Fukumoto, Kenji; Hikita, Hayato; Saito, Yoshinobu et al.
Citation	Cellular and Molecular Gastroenterology and Hepatology. 2025, 20(4), p. 101698
Version Type	VoR
URL	https://hdl.handle.net/11094/104045
rights	This article is licensed under a Creative Commons Attribution 4.0 International License.
Note	

The University of Osaka Institutional Knowledge Archive : OUKA

https://ir.library.osaka-u.ac.jp/

The University of Osaka

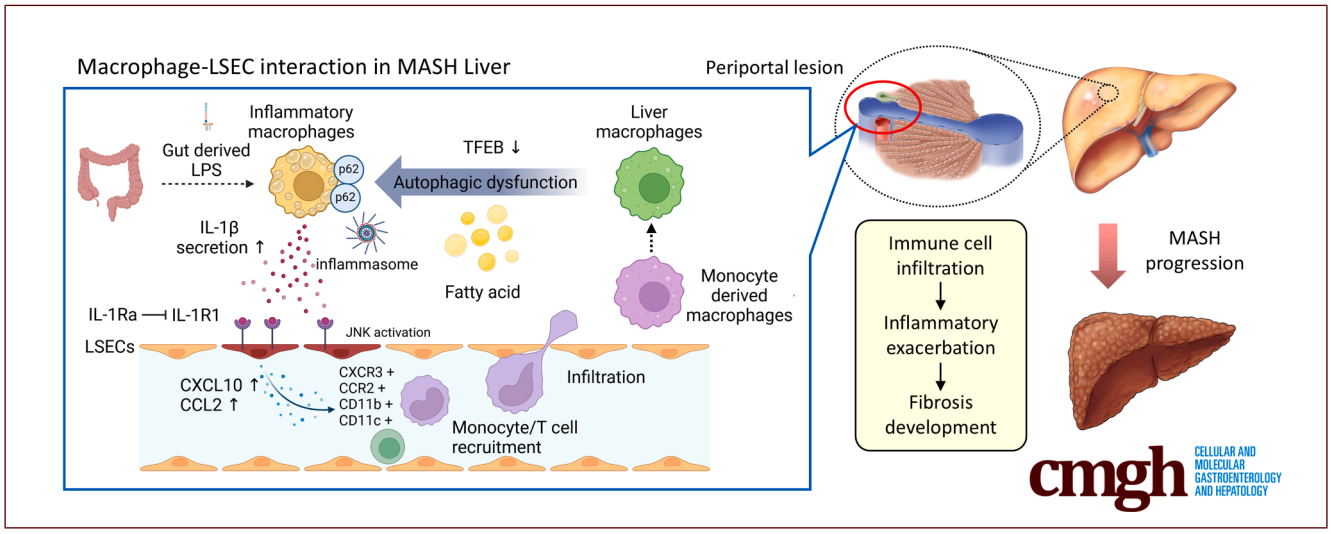
cmgh
CELLULAR AND MOLECULAR GASTROENTEROLOGY AND HEPATOLOGY

ORIGINAL RESEARCH

Liver Sinusoidal Endothelial Cells Promote Metabolic Dysfunction-associated Steatohepatitis Progression via Interleukin-1R1-mediated Chemokine Production Induced by Macrophage-derived Interleukin-1β

Kenji Fukumoto,[1] Hayato Hikita,[1] Yoshinobu Saito,[1] Yuki Makino,[1] Kazumasa Soma,[1] Seiya Kato,[1] Yoichi Sasaki,[1] Yuta Myojin,[1] Katsuhiko Sato,[1] Sadatsugu Sakane,[1] Kazuhiro Murai,[1] Yuki Tahata,[1] Takahiro Kodama,[1] Tomohide Tatsumi,[1] Daisuke Motooka,[2] Yoshiaki Kubota,[3] Shogo Kobayashi,[4] Hidetoshi Eguchi,[4] and Tetsuo Takehara[1]

[1]Department of Gastroenterology and Hepatology, The University of Osaka Graduate School of Medicine, Osaka, Japan; [2]NGS Core Facility, Research Institute for Microbial Diseases, Osaka University, Osaka, Japan; [3]Department of Anatomy, Keio University School of Medicine, Tokyo, Japan; and [4]Department of Gastroenterological Surgery, The University of Osaka Graduate School of Medicine, Osaka, Japan



SUMMARY

Macrophage-derived interleukin-1 beta activates liver endothelial cells to produce chemokines that recruit inflammatory cells and promote fibrosis. Spatial transcriptomic analysis revealed concentrated macrophage-to-endothelial signaling in periportal regions. Genetic and pharmacological blockade reduced steatohepatitis severity, highlighting this pathway as a therapeutic target.

WHAT YOU NEED TO KNOW

Background: Interleukin (IL)-1β signaling contributes to hepatic inflammation, but how macrophage-derived IL-1β interacts with endothelial and stellate cells in metabolic dysfunction-associated steatohepatitis (MASH) remains poorly understood.

Impact: CosMx spatial transcriptomics identified macrophage-to-liver sinusoidal endothelial cell IL1B–IL1R1 signaling as a dominant interaction driving C-C motif chemokine ligand 2 and C-X-C motif chemokine ligand 10 induction, linking inflammation and fibrosis in MASH.

Future Directions: Targeting IL1R1 signaling may represent a promising therapeutic approach to mitigate hepatic inflammation and fibrotic progression in MASH patients.

BACKGROUND & AIMS: Interleukin (IL)-1β is a key cytokine in hepatitis-related inflammation, but its role in metabolic dysfunction-associated steatotic liver disease (MASLD) or steatohepatitis (MASH) remains unclear. This study investigated IL-1β-mediated interactions in nonparenchymal liver cells to elucidate their contributions to pathological MASH progression.

METHODS: We used the THP-1 monocyte-derived macrophage line and TMNK-1 liver sinusoidal endothelial cell (LSEC) line for in vitro assays. Endothelial cell-specific Il1r1-knockout ($Il1r1^{\Delta EC}$) and systemic Cxcl10-knockout ($Cxcl10^{-/-}$) mice were subjected to a Western diet (WD) to establish a MASH model. An additional WD-fed cohort received the IL1R1 antagonist anakinra during the final 4 weeks. RNA sequencing data from liver tissues from patients with MASLD and spatial transcriptomic analyses focusing on nontumor regions of MASH-related hepatocellular carcinoma samples were evaluated.

RESULTS: Liver levels of mature IL-1β were elevated in WD-fed mice compared with ND-fed mice. Il1r1 was highly expressed in LSECs, and Ccl2 and Cxcl10 expression were upregulated in LSECs under WD conditions. Palmitic acid inhibited autophagy in THP-1 macrophages, increasing IL-1β secretion. IL-1β enhanced CCL2 and CXCL10 expression in TMNK-1 LSECs via JNK activation. In $Il1r1^{\Delta EC}$ and $Cxcl10^{-/-}$ mice, WD-induced inflammatory cell infiltration and fibrosis were attenuated, and anakinra produced similar effects. In human datasets, CCL2 and CXCL10 were upregulated in MASH livers and correlated with NAFLD activity scores. Spatial transcriptomics revealed a dominant periportal macrophage-to-LSEC IL1B–IL1R1 interaction that generates chemokine-enriched LSECs, forming inflammatory–fibrotic niches that facilitate immune cell recruitment.

CONCLUSIONS: Macrophage-derived IL-1β promotes hepatic inflammation and fibrosis through IL1R1-dependent chemokine induction in LSECs, highlighting IL1R1 signaling as a therapeutic target in MASH. *(Cell Mol Gastroenterol Hepatol 2026;20:101698; https://doi.org/10.1016/j.jcmgh.2025.101698)*

Keywords: Anakinra; CXCL10; IL1R1; LSEC; Macrophage; MASH; Spatial Transcriptomics.

Due to the global rise in the prevalence of obesity and type 2 diabetes, metabolic dysfunction-associated steatotic liver disease (MASLD) and metabolic dysfunction-associated steatohepatitis (MASH) have become the most common liver diseases, affecting approximately a quarter of the world's population.[1] MASH increases the risk of hepatocellular carcinoma (HCC) and is considered a systemic metabolic disorder that also increases the risk of cardiovascular complications.[2] The pathophysiology of MASH involves not only lipotoxicity but also insulin resistance, alterations in the gut microbiota, and various interactions within the liver microenvironment.[3,4] Understanding these complex mechanisms is crucial for developing effective strategies for the prevention and treatment of MASH.[5]

Interleukin (IL)-1β is a proinflammatory cytokine that plays a central role in the innate immune response. It is produced primarily by macrophages and is activated in response to the presence of pathogen-associated molecular patterns (PAMPs) and damage-associated molecular patterns (DAMPs).[6] IL-1β exerts its effects through the IL-1 receptor (IL-1R), activating the nuclear factor kappa B (NF-κB) and mitogen-activated protein kinase (MAPK) signaling pathways to amplify inflammatory responses. IL-1β has been implicated in various pathological liver conditions, such as alcoholic liver disease (ALD),[7] viral hepatitis (especially hepatitis C virus [HCV] infection),[8] and acute liver failure (ALF).[9] In ALD patients, lipopolysaccharides (LPS) derived from the gut microbiota activate liver macrophages, leading to increased IL-1β production, thereby accelerating liver damage and fibrosis. In patients with viral hepatitis, including HCV infection, viral components stimulate intrahepatic macrophages, promoting IL-1β secretion, which drives chronic inflammation and enhances fibrosis progression. Similarly, in patients with ALF, extensive hepatocyte necrosis releases DAMPs, excessively activating IL-1β signaling and contributing to uncontrolled inflammation and multiorgan failure.

In patients with MASH, alterations in the gut microbiota increase the production of LPS, which reaches liver macrophages via the portal vein and induces IL-1β secretion.[10,11] Additionally, stimulation by fatty acids and other DAMPs activates the inflammasome in liver macrophages, further increasing IL-1β production and triggering hepatitis.[12,13] However, the precise mechanisms underlying increased IL-1β secretion in patients with MASH, the specific IL-1β target cells, and the downstream liver pathology effects remain unclear. Recent advancements in single-cell

Abbreviations used in this paper: **ALD, alcoholic liver disease; ALF, acute liver failure; ALT, alanine aminotransferase; ANOVA, analysis of variance; BFM, bafilomycin; BSA, bovine serum albumin; CCL, C-C motif chemokine ligand; CXCL, C-X-C motif chemokine ligand; cDNA, complementary DNA; DAMP, damage-associated molecular pattern; DAPI, 4′,6-diamidino-2-phenylindole; DMEM, Dulbecco's modified Eagle's medium; EC, endothelial cell; ELISA, enzyme-linked immunosorbent assay; FBS, fetal bovine serum; FDA, United States Food and Drug Administration; FFPE, formalin-fixed paraffin-embedded; FOV, field of view; GTT, glucose tolerance test; H&E, hematoxylin and eosin; HCC, hepatocellular carcinoma; HCV, hepatitis C virus; HSC, hepatic stellate cell; IFN, interferon; IL, interleukin; IL-1R, interleukin-1 receptor; IL-1Ra, interleukin-1 receptor agonist; JNK, c-Jun N-terminal kinase; KC, Kupffer cell; KEGG, Kyoto Encyclopedia of Genes and Genomes; KO, knockout; LPS, lipopolysaccharide; LR, ligand-receptor; LSEC, liver sinusoidal endothelial cell; MACS, magnetic-activated cell sorting; MAPK, mitogen-activated protein kinase; MASLD, metabolic dysfunction-associated steatotic liver disease; MASH, metabolic dysfunction-associated steatohepatitis; MoMF, monocyte-derived macrophage; mRNA, messenger RNA; NAFLD, nonalcoholic fatty liver disease; NASH, nonalcoholic steatohepatitis; NC, negative control; ND, normal diet; NF-κB, nuclear factor kappa B; NPC, nonparenchymal cell; PA, palmitic acid; PAMP, pathogen-associated molecular pattern; PBS, phosphate buffered saline; PMA, phorbol 12-myristate 13-acetate; qRT-PCR, quantitative real-time reverse-transcription polymerase chain reaction; RNA-seq, RNA sequencing; ROS, reactive oxygen species; RPMI, Roswell Park Memorial Institute; SEM, standard error of the mean; TFEB, transcription factor EB; UMAP, Uniform Manifold Approximation and Projection; WD, Western diet.**

Most current article

© 2025 The Authors. Published by Elsevier Inc. on behalf of the AGA Institute. This is an open access article under the CC BY license (http://creativecommons.org/licenses/by/4.0/).

2352-345X
https://doi.org/10.1016/j.jcmgh.2025.101698

analyses have allowed researchers to gradually elucidate the roles of intrahepatic nonparenchymal cells (NPCs) in MASH, highlighting the importance of intercellular interactions.[14,15] Given the established role of IL-1β in various liver diseases, IL-1β likely contributes to MASH progression by interacting with intrahepatic NPCs to promote inflammation and fibrosis. In this study, we aimed to explore how IL-1β-mediated intercellular interactions influence the pathogenesis of MASH and contribute to disease progression.

Results

Feeding Mice a Western Diet Increases IL-1β Levels and Impairs Macrophage Autophagy in the Liver

Mice fed a Western diet (WD) presented pathological features of MASH, including fat accumulation, inflammatory cell infiltration, and liver fibrosis. Approximately 40% of these mice (7/18) developed tumors after 48 weeks (Figure 1*A*). They also exhibited weight gain, impaired glucose tolerance, and increased serum alanine aminotransferase (ALT) levels and were considered a physiological model closely resembling human MASH (Figure 1*B*). Pro-IL-1β is cleaved into its mature form, enabling its secretion. Compared with those in the normal diet (ND) group, the mature liver tissue IL-1β protein levels were increased in mice after 24 weeks of WD feeding (Figure 1*C*). In the WD group, increased levels of the autophagy-related proteins p62 and LC3-II were observed (Figure 1*C*), suggesting autophagy impairment-induced accumulation, which is consistent with previous reports.[16]

To evaluate autophagy in hepatic macrophages, a primary source of IL-1β, we measured p62 expression levels using flow cytometry. The macrophages were classified as monocyte-derived macrophages (MoMFs) ($CD45^+$ $Ly6G^-$ $Cd11b^{high}$ $F4/80^+$) or Kupffer cells (KCs) ($CD45^+$ $Ly6G^-$ $Cd11b^{int}$ $F4/80^+$). The mean fluorescence intensities of p62 expression were significantly greater in both MoMFs and KCs from livers of WD-fed mice than in those from ND-fed mice (Figure 1*D*). Conversely, the expression of the *Sqstm1* gene, which encodes p62, in liver macrophages isolated from ND- and WD-fed mice did not differ (Figure 3*J*), suggesting that WD feeding led to impaired autophagy in macrophages. The proportion of MoMFs among hepatic $CD45^+$ cells was significantly higher in WD-fed mice than in ND-fed mice. In addition, the absolute number of isolated hepatic MoMFs was also increased in WD-fed mice, indicating increased recruitment and expansion of MoMFs under MASH conditions (Figure 1*E*).

Palmitic Acid Promotes IL-1β Secretion by Impairing Macrophage Autophagy

Next, we investigated the effects of palmitic acid (PA) administration on macrophages in vitro, as PA is a key fatty acid involved in MASH pathophysiology. When PA was added to LPS-stimulated THP-1 macrophages, *IL1B* gene expression did not increase, but IL-1β secretion was increased (Figure 2*A*). IL-1β is cleaved from pro-IL-1β upon inflammasome activation.[6] Caspase-1 secretion, a marker of inflammasome activation, increased with PA treatment (Figure 2*A*). The PA-induced increase in IL-1β secretion, without changes in *IL1B* gene expression, was attenuated by treatment with Z-YVAD-FMK, a caspase-1 inhibitor (Figure 2*B*).

We investigated the involvement of autophagy in PA-induced inflammasome activation. In patients with acute hepatitis, autophagy regulates inflammation by degrading excessive inflammasomes and reactive oxygen species (ROS).[17] The addition of PA to THP-1 macrophages decreased autophagic flux, with a decrease in transcription factor EB (TFEB) levels and increases in p62 and LC3-II protein levels (Figure 2*C* and *D*), suggesting the impairment of late-stage autophagy. TFEB is a critical protein for lysosomal biogenesis,[18,19] and reduction of its expression suggests autophagy dysfunction. Treatment with the autophagy inhibitor bafilomycin (BFM) also increased IL-1β secretion and caspase-1 release (Figure 2*E*). These findings suggest that fatty acid-induced autophagy dysfunction enhances macrophage IL-1β secretion through inflammasome activation.

Inflammatory Chemokine Expression Is Upregulated in the LSECs of Experimental MASH Mice

The single-cell analysis of the livers of wild-type mice fed an ND (n = 2) or a WD (n = 1) for 12 weeks revealed 19 cell clusters, including 4 macrophage clusters (Figure 3*A*, *B*). *Il1b* was highly expressed in macrophages and neutrophils, whereas its receptor, *Il1r1*, was highly expressed in liver sinusoidal endothelial cells (LSECs) and hepatic stellate cells (HSCs) (Figure 3*C*). Based on the total expression levels in WD-fed mice, in which *Il1b* expression was highest in macrophages and *Il1r1* expression was highest in LSECs (Figure 3*D*), we focused on the interaction between these cells. In LSECs, the total expression levels of genes listed in the Kyoto Encyclopedia of Genes and Genomes (KEGG) IL1-IL1R- c-Jun N-terminal kinase (JNK) signaling pathway (N00188) were calculated, and the enrichment scores were compared. The results revealed higher scores in the WD group than in the ND group (Figure 3*E*). In the cells of the LSEC clusters (LSEC 1–4), the top 10 genes with the lowest adjusted *P* values whose expression was upregulated by more than 2-fold in the WD group compared with that of the ND group included the lipid metabolism-related genes *Cd36* and *Fabp4*, as well as the inflammatory chemokine *Cxcl10* (Figure 3*F*). The expression levels of the inflammatory chemokines *Cxcl10*, *Cxcl9*, and *Ccl2* were increased among Cxcl and Ccl family genes (Figure 3*G*). LSECs were isolated from mouse liver tissues using magnetic-activated cell sorting (MACS) to validate the increased expression levels of these chemokines (Figure 3*H*). Although no difference in *Il1r1* gene expression was observed between groups, the expression of the *Ccl2*, *Cxcl9*, and *Cxcl10* genes was confirmed to be upregulated in the LSECs isolated from the WD group compared with those from the ND group (Figure 3*I*).

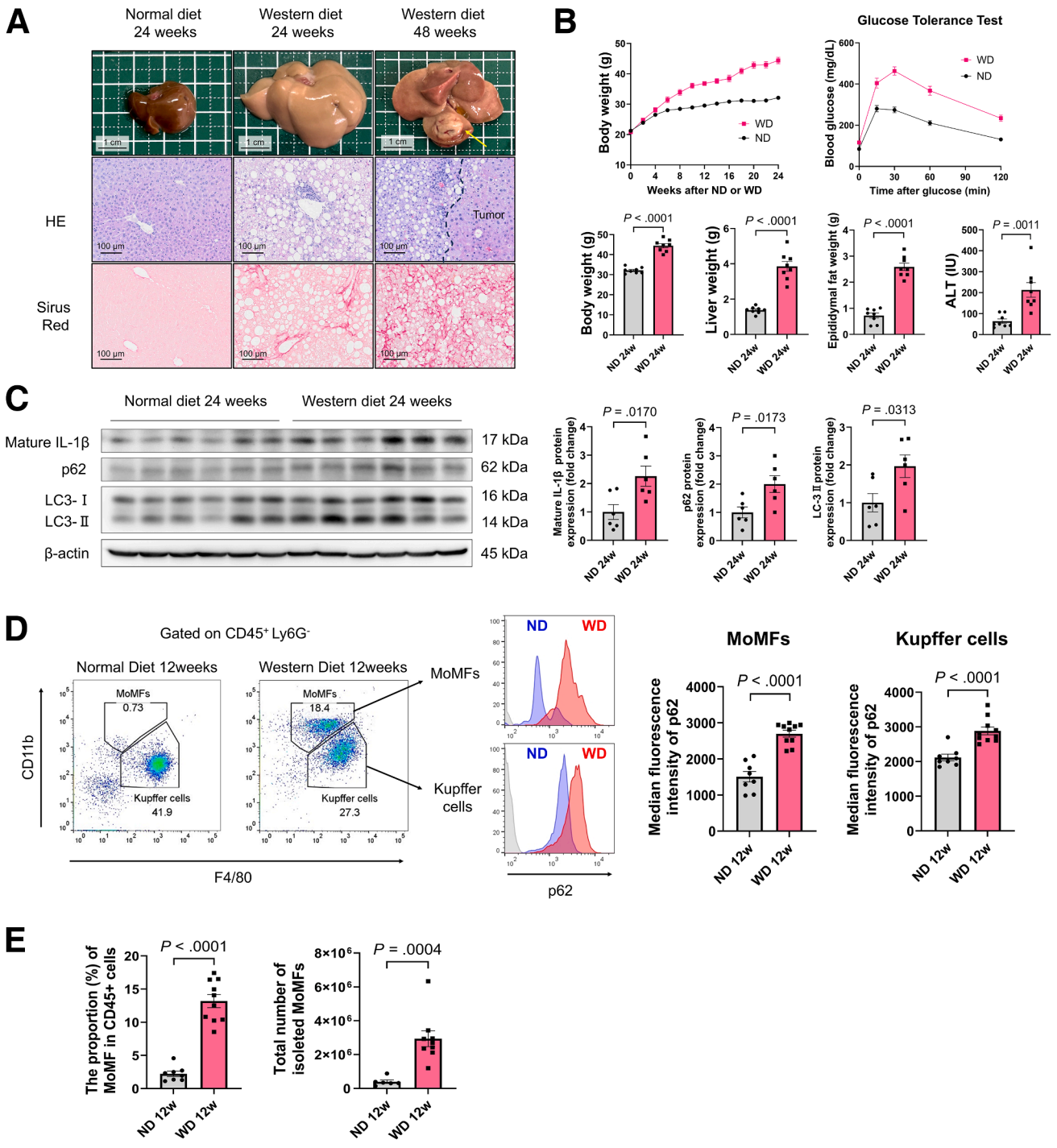


Figure 1. WD-induced MASH impairs autophagy in hepatic macrophages and increases mature IL-1β levels in liver tissue. (*A*) Histological analysis of liver tissue from a mouse model of MASH induced by ND or WD administration. (*B*) Phenotypic characteristics of mice fed an ND or WD (n = 8/group), with a GTT conducted at 24 weeks (n = 12/group). (*C*) Mature IL-1β and autophagy-related proteins in the liver tissues of mice were evaluated using Western blotting. (*D*) The median fluorescence intensity (MFI) of p62 in liver macrophages (MoMFs and KCs) from mice fed an ND or WD for 12 weeks (n = 8–10 mice/group) was analyzed using flow cytometry. (*E*) (*Left panel*) The proportion of MoMFs among CD45-positive liver cells was compared between ND- and WD-fed mice (n = 8–10 mice/group). (*Right panel*) The total number of isolated MoMFs was calculated based on the yield of NPCs obtained from each liver (n = 6–9 mice/group).

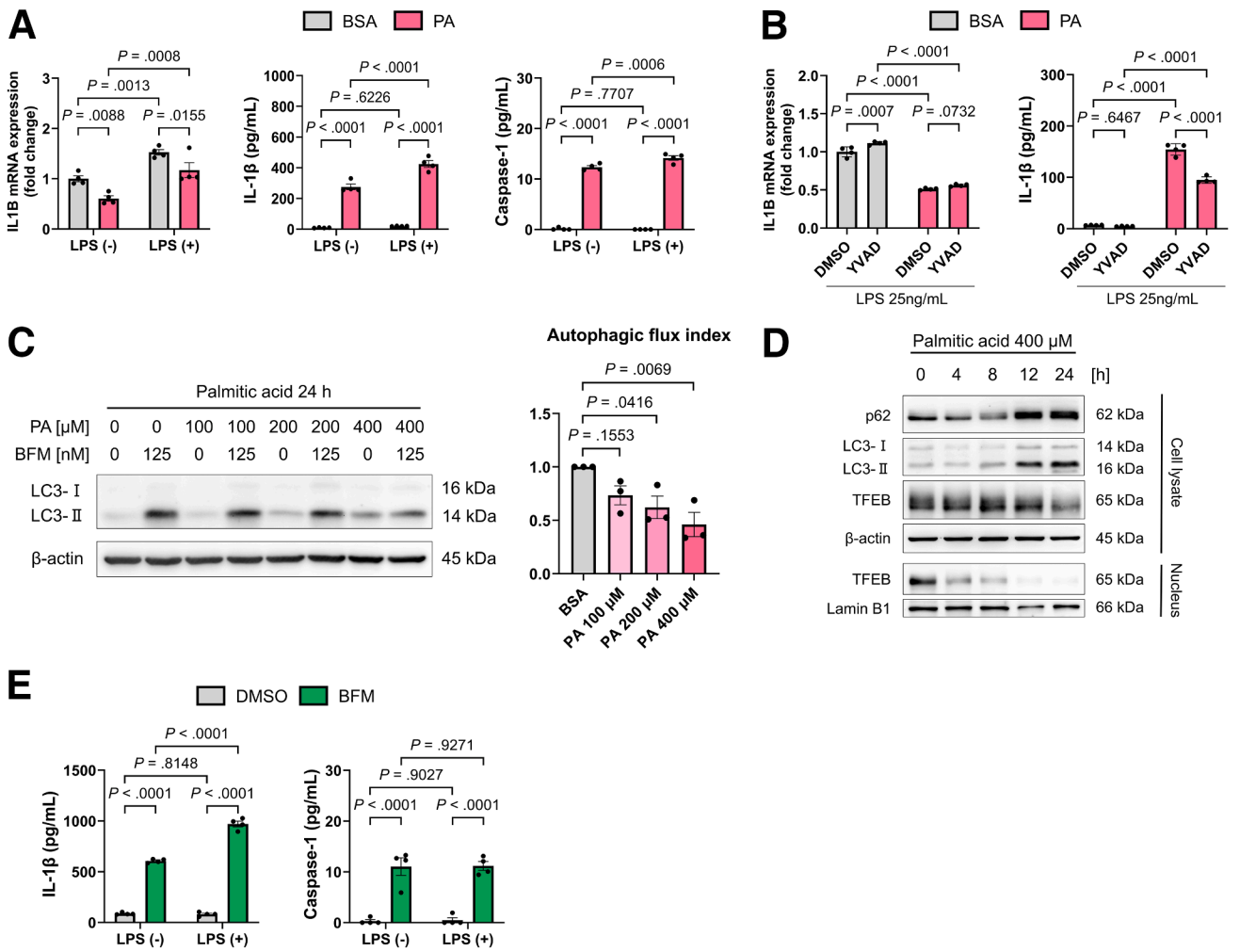
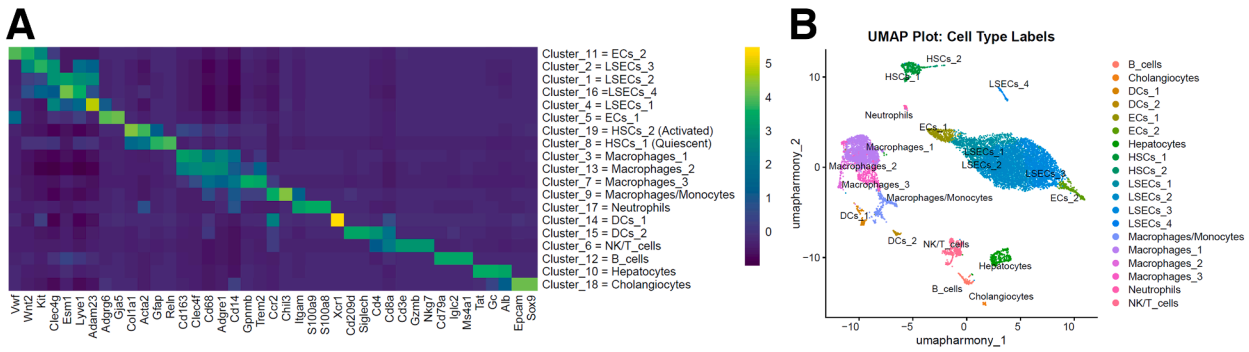


Figure 2. The impairment of autophagy in macrophages by fatty acids increases IL-1β secretion. (*A*) IL1B gene expression and the concentrations of IL-1β and caspase-1 in the supernatants of THP-1 macrophages cultured for 24 hours with or without LPS (25 ng/mL) and treated with either BSA or 400 μM PA (n = 4/group). (*B*) *IL1B* gene expression and the concentrations of IL-1β in the supernatants of THP-1 macrophages cultured for 24 hours with BSA or 400 μM PA and 25 ng/mL LPS in the presence or absence of 50 μM Z-YVAD-FMK (n = 4/group). (*C*) LC3 turnover assay to evaluate autophagic flux in THP-1 macrophages treated with PA and BFM (n = 3/group). (*D*) Expression of autophagy-related proteins in THP-1 macrophages treated with PA. (*E*) IL-1β and caspase-1 concentrations in the supernatants of THP-1 macrophages cultured for 24 hours with or without 25 ng/mL LPS and treated with either dimethyl sulfoxide (DMSO) or 50 nM BFM.

IL-1β From Macrophages Increases CCL2 and CXCL10 Expression in LSECs Through JNK Activation

Next, we investigated macrophage–LSEC interactions in vitro, focusing on their roles in MASH pathogenesis. Because impaired macrophage autophagy is thought to occur in individuals with MASH (Figures 1*D*, 2*C* and 2*D*), we first generated THP-1 cells in which the autophagy gene *ATG7* was knocked out (Figure 4*A*). Similar to the effects of PA and BFM administration (Figures 2*A*, 2*B* and 2*E*), the ATG7 knockout (KO)-induced autophagy disruption led to increased IL-1β secretion in THP-1 macrophages, along with increased caspase-1 secretion (Figure 4*B*). Human LSEC (TMNK-1) cells were cultured with the conditioned medium from LPS-stimulated THP-1 macrophages to assess the effect of macrophage-derived soluble factors on LSECs (Figure 4*C*). The conditioned medium from macrophages increased the expression of *CCL2* and *CXCL10* in TMNK-1 cells and activated p38 MAPK and JNK (Figure 4*D* and *E*). These effects were further enhanced when ATG7 expression was knocked out in macrophages (Figure 4*D* and *E*). The increased expression of *CCL2* and *CXCL10* in TMNK-1 cells cultured with ATG7-KO macrophage conditioned medium was markedly suppressed by the addition of an IL-1 receptor antagonist (IL-1Ra) (Figure 4*F*). These findings suggest that IL-1β, whose secretion was increased due to impaired autophagy induced by macrophage-conditioned medium, is the main driver of the increased chemokine expression in TMNK-1 cells. Furthermore, administration of a JNK inhibitor suppressed the expression of both *CCL2* and *CXCL10*, whereas the administration of a p38 MAPK inhibitor specifically suppressed *CXCL10* gene expression,


A
Cluster_11 = ECs_2
Cluster_2 = LSECs_3
Cluster_1 = LSECs_2
Cluster_16 =LSECs_4
Cluster_4 = LSECs_1
Cluster_5 = ECs_1
Cluster_19 = HSCs_2 (Activated)
Cluster_8 = HSCs_1 (Quiescent)
Cluster_3 = Macrophages_1
Cluster_13 = Macrophages_2
Cluster_7 = Macrophages_3
Cluster_9 = Macrophages/Monocytes
Cluster_17 = Neutrophils
Cluster_14 = DCs_1
Cluster_15 = DCs_2
Cluster_6 = NK/T_cells
Cluster_12 = B_cells
Cluster_10 = Hepatocytes
Cluster_18 = Cholangiocytes
Vwf Wnt2 Kit Clec4g Esm1 Lyve1 Adam23 Adgrg6 Gja5 Col1a1 Acta2 Glep Reln Cx3cl1 Clec4f Cd68 Adgre1 Cd14 Gpnmb Trem2 Ccr2 Chil3 Itgam S100a9 S100a8 Xcr1 Cd209d Siglech Cd4 Cd8a Cd3e Gzmb Nkg7 Cd79a Igjc2 Ms4a1 Tat Gc Alb Epcam Sox9
B
UMAP Plot: Cell Type Labels
HSCs_2
HSCs_1
LSECs_4
Neutrophils
ECs_1
Macrophages_1
LSECs_1
LSECs_2
LSECs_3
Macrophages_2
Macrophages_3
Macrophages/Monocytes
ECs_2
DCs_1
DCs_2
NK/T_cells
Hepatocytes
B_cells
Cholangiocytes
umapharmony_1
umapharmony_2
B_cells
Cholangiocytes
DCs_1
DCs_2
ECs_1
ECs_2
Hepatocytes
HSCs_1
HSCs_2
LSECs_1
LSECs_2
LSECs_3
LSECs_4
Macrophages/Monocytes
Macrophages_1
Macrophages_2
Macrophages_3
Neutrophils
NK/T_cells
C
Il1b expression
Il1r1 expression
Neutrophils
Macrophages
HSCs
Ecs / LSECs
umapharmony_1
umapharmony_2
D
total_Il1b
total_Il1r1
Total Expression (Sum of Expression)
Macrophages_1 Macrophages_2 Macrophages_3 Macrophages/Monocytes NK/T_cells B_cells Neutrophils ECs_1 ECs_2 LSECs_1 LSECs_2 LSECs_3 LSECs_4 HSCs_1 HSCs_2 DCs_1 DCs_2
E
Gene Expression of IL1R1-JNK Pathway Genes in LSECs
Fos 2.87 2.74 3.19
Jun 2.72 2.79 3.14
Irak1 0.63 0.58 0.64
Tab2 0.52 0.51 0.59
Map3k7 0.33 0.32 0.33
Mapk9 0.25 0.29 0.27
Il1r1 0.21 0.20 0.32
Map2k7 0.23 0.21 0.22
Mapk8 0.18 0.19 0.21
Map2k4 0.19 0.17 0.19
Myd88 0.16 0.18 0.19
Irak4 0.14 0.14 0.14
Traf6 0.15 0.12 0.11
Tab3 0.03 0.03 0.03
Tab1 0.02 0.01 0.01
Il1rap 0.01 0.01 0.01
ND1 ND2 WD1
Expression
Enrichment Scores for IL1R1-JNK Pathway Genes in LSEC Cells
P = 8.2e-43
Enrichment Score
Group
ND WD
group
ND
WD
F
Top 10 genes upregulated in LSECs in the WD group
Log2_FC adj_pval
Cd36 1.043 7.40E-225
Fabp4 1.349 4.35E-166
Cxcl10 1.209 2.32E-154
Nfkbiz 1.495 9.00E-111
Atf3 1.637 1.81E-97
Ednrb 1.842 5.14E-87
Klf6 1.138 3.43E-69
Flrt2 1.717 5.62E-66
Armcx4 1.805 1.31E-64
Scd1 2.523 3.68E-58
Abca1 1.066 1.45E-56
G
Gene Expression of CCl and CXCL family Genes in LSECs
Cxcl10 1.29 1.18 2.28
Cxcl9 0.49 0.72 0.91
Cxcl16 0.83 0.78 0.68
Cxcl1 0.12 0.10 0.12
Ccl2 0.04 0.03 0.09
Cxcl2 0.02 0.01 0.04
Cxcl12 0.05 0.01 0.04
Ccl5 0.01 0.01 0.02
Ccl3 0.00 0.01 0.01
Ccl4 0.00 0.01 0.01
Ccl25 0.01 0.01 0.01
Ccl24 0.00 0.01 0.00
Ccl7 0.00 0.00 0.00
Cxcl14 0.00 0.00 0.00
Ccl8 0.00 0.00 0.00
Ccl19 0.00 0.00 0.00
Ccl11 0.00 0.00 0.00
Ccl17 0.00 0.00 0.00
Cxcl13 0.01 0.01 0.00
ND1 ND2 WD1
Expression
H
<MACS: CD146 positive selection>
<MACS: F4/80 positive selection>
Liver NPC isolation
CD146+ LSECs
CD146- NPCs
F4/80+ Liver macrophages
Other NPCs
Alb mRNA expression (fold change)
Lyve1 mRNA expression (fold change)
Adgre1 mRNA expression (fold change)
P < .0001
Hepatocytes LSECs Macrophages
I
Il1r1 mRNA expression (fold change)
P = .3384
Ccl2 mRNA expression (fold change)
P = .0004
Cxcl9 mRNA expression (fold change)
P = .0419
Cxcl10 mRNA expression (fold change)
P = .0023
ND 24w WD 24w
LSECs
J
Sqstm1 mRNA expression (fold change)
P = .6859
Il1b mRNA expression (fold change)
P = .4428
ND 24w WD 24w
Liver Macrophages

indicating that the JNK and p38 MAPK pathways downstream of IL1R1 are involved (Figure 4*F*). Recombinant human IL-1β was added to TMNK-1 cells to further investigate this pathway, and increased expression of the *CCL2* and *CXCL10* genes was observed (Figure 4*G*). This effect was suppressed by administration of the JNK and p38 MAPK inhibitors (Figure 4*H*).

Mice with bone marrow-derived cell-specific Atg7 KO (LysM-Cre Atg7$^{flox/flox}$ [Atg7$^{\Delta Mye}$] mice) or control mice (Atg7$^{flox/flox}$ mice) were intraperitoneally injected with LPS to examine the effect of impaired macrophage autophagy on *CCL2* and *CXCL10* expression in LSECs in vivo (Figure 5*A*). Atg7$^{\Delta Mye}$ mice presented decreased *Atg7* expression in liver macrophages but no changes in its expression in LSECs (Figure 5*B*). Compared with Atg7$^{flox/flox}$ mice, Atg7$^{\Delta Mye}$ mice presented increased IL-1β levels in the liver (Figure 5*A*). The expression levels of *Ccl2* and *Cxcl10* were higher in the whole liver and LSECs from Atg7$^{\Delta Mye}$ mice than in those from the Atg7$^{flox/flox}$ mice (Figure 5*C* and *D*).

Endothelial Cell-specific Il1r1*-KO Alleviates Liver Fibrosis and Inflammatory Cell Infiltration in MASH-affected Livers and Reduces* CCL2 *and* CXCL10 *Expression in LSECs*

To investigate the impact of IL-1β on MASH pathogenesis via LSECs, we fed a WD to tamoxifen-inducible endothelial cell (EC)-specific Il1r1-KO mice (Cdh5-Cre^{ERT2} Il1r1$^{flox/flox}$, Il1r1$^{\Delta EC}$). Compared with Il1r1$^{flox/flox}$ mice, Il1r1$^{\Delta EC}$ mice consumed more food and tended to weigh more (Figure 6*A*). No significant difference in ALT levels was observed between groups (Figure 6*A*), but immunohistochemical staining showed that the CD3e- and CD11b-positive liver areas were reduced in Il1r1$^{\Delta EC}$ mice (Figure 6*B*). Additionally, the expression levels of *Ccl2*, *Cxcl10*, and monocyte/macrophage-related genes in liver tissues were lower in Il1r1$^{\Delta EC}$ mice than in Il1r1$^{flox/flox}$ mice (Figure 6*C*). Moreover, the Sirius red-positive area and the expression of fibrosis-related genes in liver tissues were reduced in Il1r1$^{\Delta EC}$ mice (Figure 6*B*), indicating the attenuation of inflammation and fibrosis in experimental MASH mice.

Il1r1 expression was suppressed in LSECs isolated from Il1r1$^{\Delta EC}$ mice using MACS (Figure 6*D*). Additionally, the expression levels of *Ccl2* and *Cxcl10* were lower in Il1r1$^{\Delta EC}$ mice than in Il1r1$^{flox/flox}$ mice (Figure 6*D*). The expression of genes related to the IL-1β–IL1R1–JNK pathway, such as *Fos* and *Jun*, was reduced in the Il1r1$^{\Delta EC}$ mice (Figure 6*D*), suggesting that this reduction may be involved in the downregulation of inflammatory chemokine expression.

Cxcl10-KO Alleviates Liver Fibrosis and Inflammatory Cell Infiltration in MASH-affected Livers

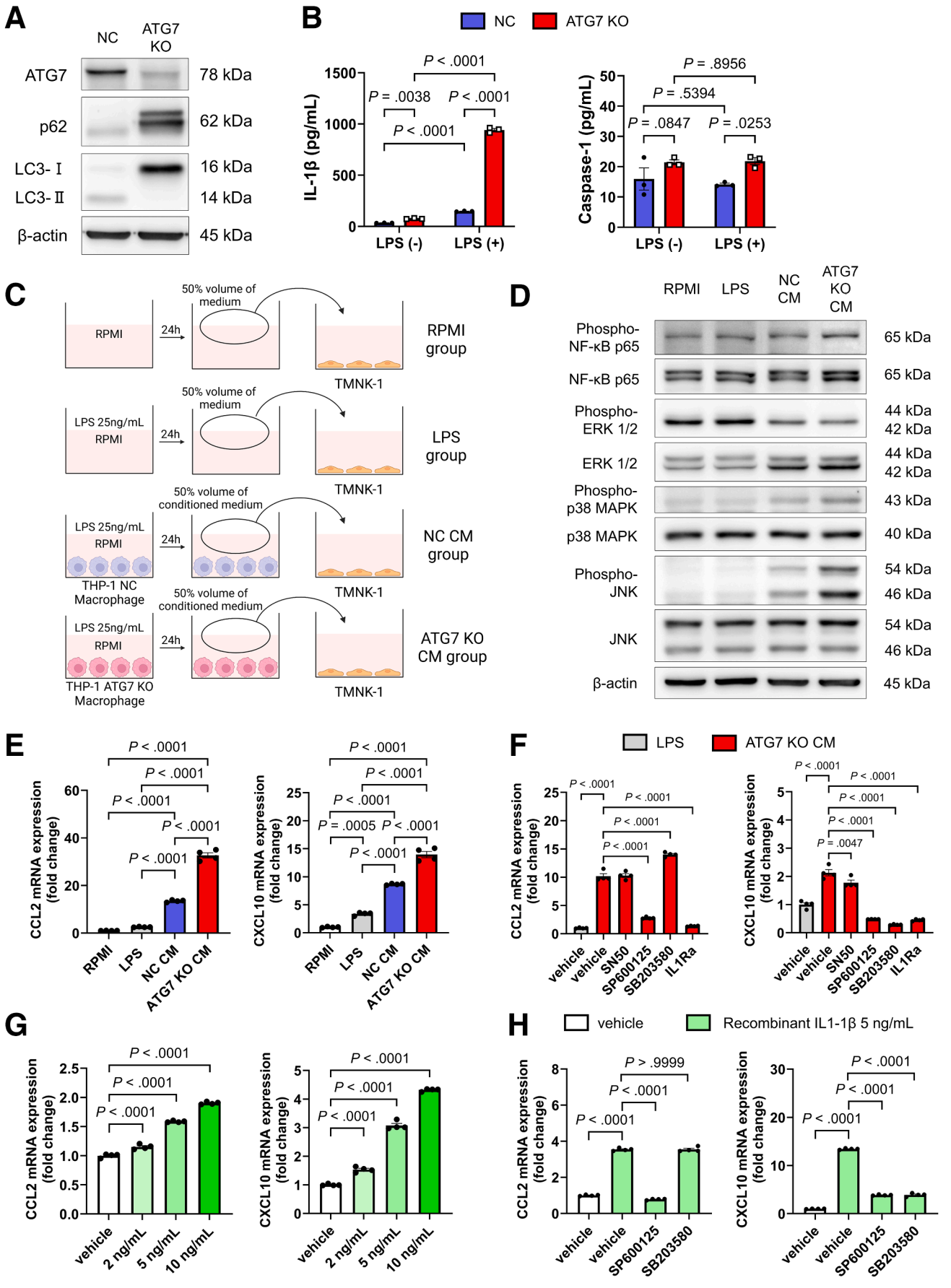
To investigate the impact of Cxcl10 signaling on MASH pathogenesis, we fed a WD to systemic Cxcl10-KO mice (Cxcl10$^{-/-}$ mice). The expression levels of *Cxcl10* were completely inhibited even after WD feeding (Figure 7*A*). After WD feeding, Cxcl10$^{-/-}$ mice presented no differences in body weights or liver weights, but their ALT levels were lower than those of wild-type mice (Figure 7*B*). Compared with those in wild-type mice, the CD3e- and CD11b-positive liver areas were reduced in Cxcl10$^{-/-}$ mice (Figure 7*C*). The hepatic expression levels of macrophage/monocyte-related genes were lower in Cxcl10$^{-/-}$ mice than in WT mice (Figure 7*D*). Additionally, the Sirius red-positive area and the expression of fibrosis-related genes in liver tissues were also decreased in Cxcl10$^{-/-}$ mice (Figure 7*C* and *D*).

To examine the effect of Cxcl10 on monocytes, we administered recombinant human CXCL10 to THP-1 cells. Recombinant human CXCL10 increased the migratory ability of THP-1 cells, suggesting that CXCL10 may mobilize monocytes (Figure 7*E*). These findings suggest that LSEC-derived CXCL10 may contribute to the progression of MASH pathology by recruiting immune cells, including monocytes.

IL1R1 Blockade With Anakinra Attenuates Hepatic Inflammation and Fibrosis in Mice With Established MASH

We administered the IL1R1 antagonist anakinra to mice during the final 4 weeks of WD feeding to further evaluate the therapeutic relevance of IL-1β–IL1R1 signaling in established MASH (Figure 8*A*). No differences in body weight or baseline serum ALT levels were observed between groups prior to treatment. After treatment, anakinra-treated mice showed modest reductions in CD11b- and CD3e-positive areas in the liver, accompanied by a trend toward decreased Sirius red-positive fibrosis (Figure 8*B*). Consistent with these histological findings, hepatic expression of inflammatory chemokine genes, including *Ccl2* and *Cxcl10*, and monocyte/macrophage-related genes such as *Itgam*, was reduced following anakinra treatment (Figure 8*C*). The expression of fibrosis-related genes, including Tgfb1, was also downregulated (Figure 8*C*).

Figure 3. (***See previous page***). **Inflammatory chemokine expression is upregulated in the LSECs of WD-fed mice.** (*A*–*G*) Single-cell RNA-seq of liver tissues from wild-type mice fed an ND (n = 2) and a WD (n = 1). (*A*) A heatmap of clusters and representative marker genes used for cell type identification. (*B*) Cell types according to UMAP. (*C*) The gene expression of *Il1b* and *Il1r1* on the UMAP, combining the ND and WD groups. (*D*) A bar graph showing the total *Il1r1* or *Il1b* expression summed across all cells of each cell type in NPCs from the WD group. (*E*) A heatmap comparing the expression levels of genes listed in the KEGG IL1-IL1R-JNK signaling pathway (N00188) in LSECs between samples (*left*), and a violin plot comparing the enrichment scores calculated based on the total expression levels of those genes between groups (*right*). The bars on the plot represent the mean. (*F*) Top 10 upregulated genes in LSECs in the WD group compared with the ND group ranked by *P* value. (*G*) A heatmap of inflammatory chemokine gene expression in LSECs of each mouse. (*H*) Isolation of LSECs and macrophages from ND-fed mice liver by MACS and purity assessment by RT-qPCR (n = 12/group). (*I* and *J*) Gene expression in isolated LSECs (*I*) and liver macrophages (*J*) (n = 12/group).


A
NC
ATG7 KO
ATG7
p62
LC3- I
LC3- II
β-actin
78 kDa
62 kDa
16 kDa
14 kDa
45 kDa
B
NC
ATG7 KO
IL-1β (pg/mL)
Caspase-1 (pg/mL)
LPS (-)
LPS (+)
C
RPMI
LPS 25ng/mL
50% volume of medium
50% volume of conditioned medium
24h
TMNK-1
THP-1 NC Macrophage
THP-1 ATG7 KO Macrophage
RPMI group
LPS group
NC CM group
ATG7 KO CM group
D
RPMI
LPS
NC CM
ATG7 KO CM
Phospho-NF-κB p65
NF-κB p65
Phospho-ERK 1/2
ERK 1/2
Phospho-p38 MAPK
p38 MAPK
Phospho-JNK
JNK
β-actin
65 kDa
44 kDa
42 kDa
43 kDa
40 kDa
54 kDa
46 kDa
E
CCL2 mRNA expression (fold change)
CXCL10 mRNA expression (fold change)
F
LPS
ATG7 KO CM
vehicle
SN50
SP600125
SB203580
IL1Ra
G
2 ng/mL
5 ng/mL
10 ng/mL
H
vehicle
Recombinant IL1-1β 5 ng/mL

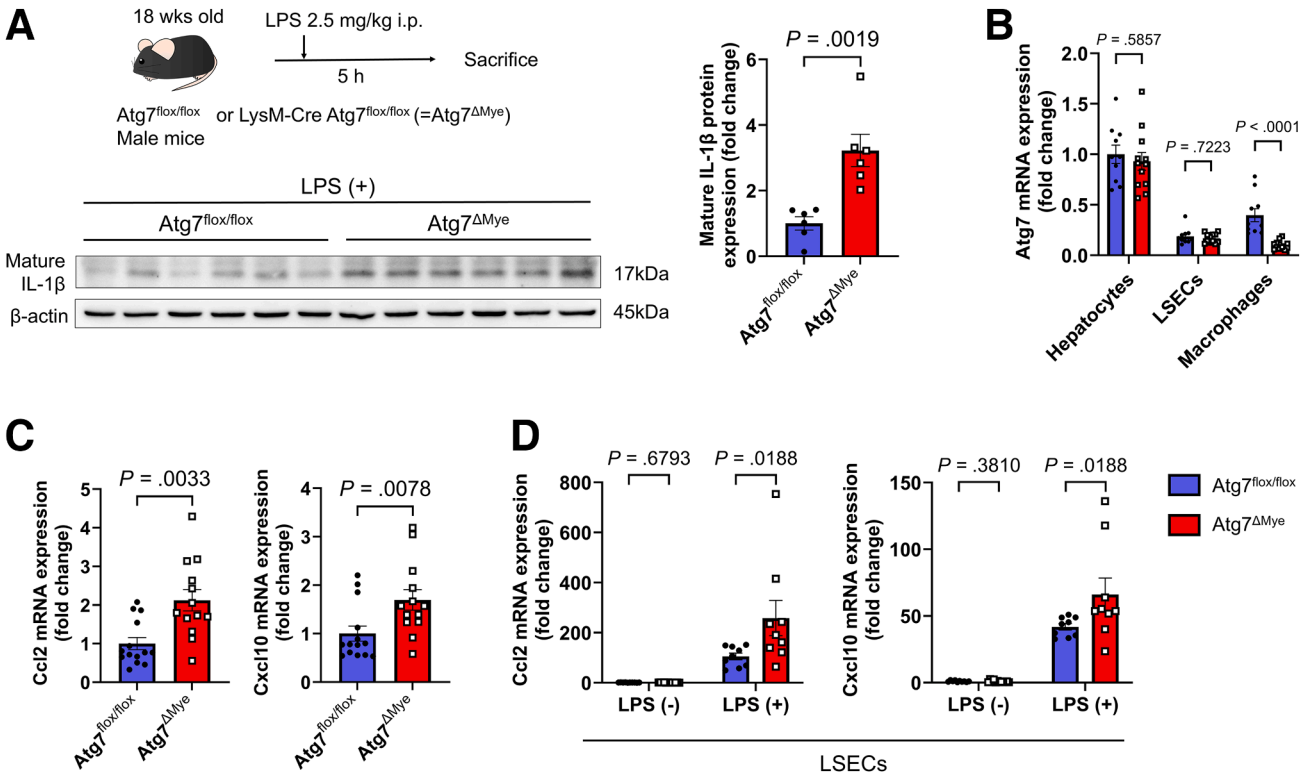


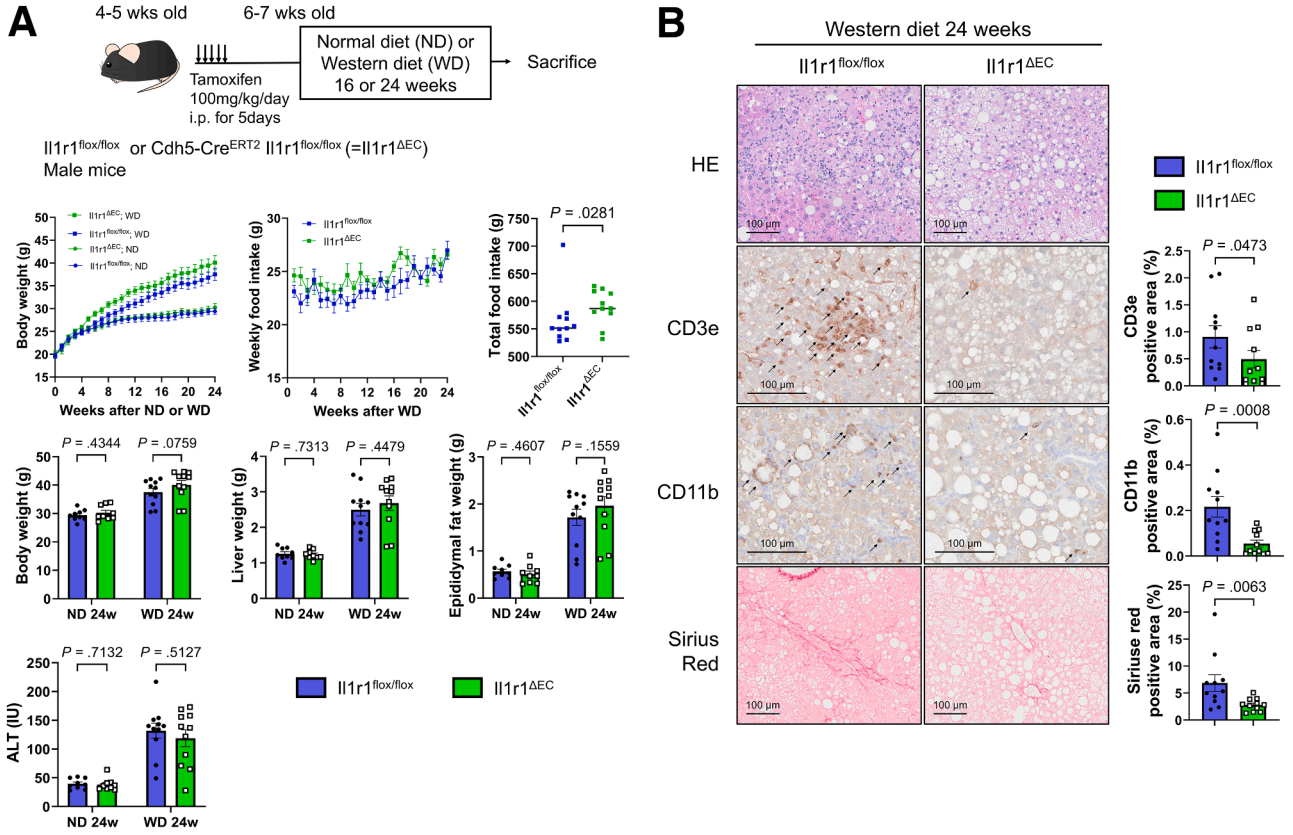
Figure 5. Myeloid-specific Atg7 deficiency is associated with increased levels of mature IL-1β in liver tissue and increased chemokine expression in LSECs. (*A*) Evaluation of mature IL-1β protein levels in liver tissues from Atg7$^{flox/flox}$ or Atg7$^{\Delta Mye}$ mice in LPS intraperitoneal injection model mice (n = 6/group). (*B*) Atg7 gene expression in cells isolated from liver tissues of Atg7$^{flox/flox}$ or Atg7$^{\Delta Mye}$ mice (n = 10–12/group). (*C*) Expression of inflammatory chemokine genes in liver tissues from model mice intraperitoneally injected with LPS (n = 13–14 mice/group). (*D*) Expression of inflammatory chemokine genes in isolated LSECs (n = 9–12/group).

These results support the hypothesis that IL1R1 signaling contributes to immune cell recruitment and fibrotic progression during MASH and suggest that pharmacological IL1R1 blockade may represent a potential therapeutic strategy.

The Expression Levels of Inflammatory Chemokines Are Increased in the Livers of Patients With MASH

We investigated the correlation between the expression of CXCL10 and other inflammation-related genes and disease progression in patients with MASLD. The RNA sequencing data from 98 patients with MASLD (GSE167523), which we previously reported,[20] revealed that expression of *CCL2* and *CXCL10*, as well as that of monocyte/macrophage marker genes such as *ITGAM* and *ITGAX*, was upregulated in the MASH group compared with the non-MASH group (Figure 9*A*). Furthermore, among the CCL and CXCL family members whose expression was upregulated in the MASH group, the top genes with the lowest adjusted *P* values were CXCL10 and CCL2 (Figure 9*B*). The enrichment analysis revealed that the activation of pathways related to chemokines and cell migration was upregulated in the MASH group (Figure 9*C*). The expression of the *ITGAM* and *ITGAX* genes was positively correlated with *CXCL10* expression (Figure 9*D*). The expression of these inflammation-related genes increased

Figure 4. (***See previous page***). **Increased IL-1β secretion by macrophages due to autophagy impairment enhances inflammatory chemokine expression in LSECs.** (*A*) Protein expression in ATG7-KO macrophages and NC macrophages generated using the CRISPR-CAS9 system. (*B*) Evaluation of IL-1β and caspase-1 levels in the culture supernatant of THP-1 macrophages by ELISA following 24-hour stimulation with or without 25 ng/mL LPS (n = 3/group). (*C*) Experimental method using LPS-stimulated THP-1 macrophage conditioned medium. (*D*) Evaluation of NF-κB or MAP kinase-related proteins in TMNK-1 cells. (*E* and *F*) Inflammatory chemokine gene expression in TMNK-1 cells when treated with control medium or THP-1 macrophage conditioned medium (n = 4/group). SN50, NF-κB inhibitor; SP600125, JNK inhibitor; SB203580, p38 MAPK inhibitor. (*G*) Inflammatory chemokine gene expression measured 24 hours after treating TMNK-1 cells with varying concentrations of human recombinant IL-1β (n = 4/group). (*H*) Evaluation of inflammatory chemokine expression in TMNK-1 cells after 6 hours of stimulation with recombinant human IL-1β (5 ng/mL) in the presence of SP600125 and SB203580 (n = 4/group).


A
4-5 wks old
6-7 wks old
Normal diet (ND) or Western diet (WD) 16 or 24 weeks
Sacrifice
Tamoxifen 100mg/kg/day i.p. for 5days
Il1r1flox/flox or Cdh5-CreERT2 Il1r1flox/flox (=Il1r1ΔEC) Male mice
Body weight (g)
Weeks after ND or WD
Weekly food intake (g)
Weeks after WD
Total food intake (g)
P = .0281
Body weight (g)
P = .4344
P = .0759
ND 24w
WD 24w
Liver weight (g)
P = .7313
P = .4479
Epididymal fat weight (g)
P = .4607
P = .1559
ALT (IU)
P = .7132
P = .5127
Il1r1flox/flox
Il1r1ΔEC
B
Western diet 24 weeks
Il1r1flox/flox
Il1r1ΔEC
HE
CD3e
CD11b
Sirius Red
100 μm
CD3e positive area (%)
P = .0473
CD11b positive area (%)
P = .0008
Siriuse red positive area (%)
P = .0063
C
Inflammatory chemokines
Ccl2 mRNA expression (fold change)
P = .0056
P = .0233
Cxcl10 mRNA expression (fold change)
P = .1359
P = .0451
Fibrosis-related genes
Col1a1 mRNA expression (fold change)
P > .9999
P = .0093
Tgfb1 mRNA expression (fold change)
P = .1476
P = .0059
Macrophage/Monocyte-related genes
Itgam mRNA expression (fold change)
P = .3114
P = .0163
Itgax mRNA expression (fold change)
P = .5457
P = .0052
Ccr2 mRNA expression (fold change)
P = .0625
P = .0079
Cxcr3 mRNA expression (fold change)
P = .2224
P = .0068
D
Il1r1 mRNA expression (fold change)
P < .0001
Fos mRNA expression (fold change)
P = .0005
Jun mRNA expression (fold change)
P = .0115
Ccl2 mRNA expression (fold change)
P = .0002
Cxcl10 mRNA expression (fold change)
P = .0029
LSECs

with increasing nonalcoholic fatty liver disease (NAFLD) activity scores (Figure 9*E*). These findings suggest that the increased expression of inflammatory chemokines, including CXCL10, and the increased infiltration of MoMFs play crucial roles in the progression of MASH pathology.

Spatial Transcriptomics Identifies Periportal Macrophage–LSEC IL1B–IL1R1 Signaling as a Dominant Inflammatory–Fibrotic Interaction in Patients With MASH

We performed a high-resolution spatial transcriptomic analysis of surgically excised liver tissues from 2 patients with MASH-related HCC using CosMx to further characterize intercellular communication in MASH. In the first patient (CosMx_MASH_sample_1), cells were segregated into multiple major cell clusters, including 3 endothelial cell/LSEC subsets (ECs_and_LSECs_1–3) (Figure 10*A*). We first calculated directional spatial proximity scores between all cell type pairs to quantify the likelihood of physical adjacency (Figure 10*B*). Based on these proximity matrices, we then computed spatially weighted ligand-receptor (LR) scores for 364 one-to-one LR pairs by integrating ligand/receptor expression levels with source → target proximity. Among all cell type combinations, LR pairs enriched in macrophage → endothelial cell/LSEC interactions were identified, and IL1B–IL1R1 emerged as one of the top enriched pairs (Figure 10*C*). Spatial LR heatmaps further showed that IL1B–IL1R1 signaling was particularly pronounced from macrophages to the ECs_and_LSECs_2 subset (Figure 10*D*). Notably, this endothelial subset expressed CCL2 and CXCL10 at high levels, similar to HSCs and cholangiocytes, suggesting a potential role in recruiting MoMFs, T cells, and B cells.

The spatial distance analysis further revealed that periportal endothelial subsets (ECs_and_LSECs_1/2) resided significantly closer to cholangiocytes than the pericentral ECs_and_LSECs_3 subset (Figure 10*E*). Periportal ECs exhibited a greater abundance of neighboring macrophages within a 20-μm radius (Figure 10*F*), suggesting greater opportunities for paracrine stimulation. The neighborhood (niche) analysis identified periportal niches enriched for inflammatory and fibrotic signatures that were characterized by the accumulation of MoMFs, inflammatory T cells, and elevated expression of the CCL2, CXCL10, ITGAM, CCR2, and COL1A1 transcripts (Figure 11*A*–*E*). These results indicate that periportal interaction zones represent spatially organized inflammatory–fibrotic microenvironments driven by IL1B–IL1R1 signaling.

We next examined whether these findings were reproducible in an independent MASH sample (CosMx_MASH_sample_2) (Figure 12*A*). Consistent with the first sample, macrophage → endothelial/LSEC LR interactions were again strongly enriched, with IL1B–IL1R1 emerging as a top spatially weighted pair (Figure 12*B* and *C*). Chemokine-mediated signaling from EC/LSEC subsets toward MoMFs (eg, CCL2–CCR2) was also detected (Figure 12*C*). Periportal endothelial subsets were localized close to cholangiocytes and exhibited increased macrophage proximity (Figure 12*D* and *E*). The neighborhood analysis similarly identified periportal niches enriched for MoMFs and inflammatory–fibrotic gene signatures (Figure 12*F*–*J*). These results validate that macrophage-derived IL-1β stimulates periportal LSECs through IL1R1, reinforcing chemokine-driven inflammatory–fibrotic niches in MASH.

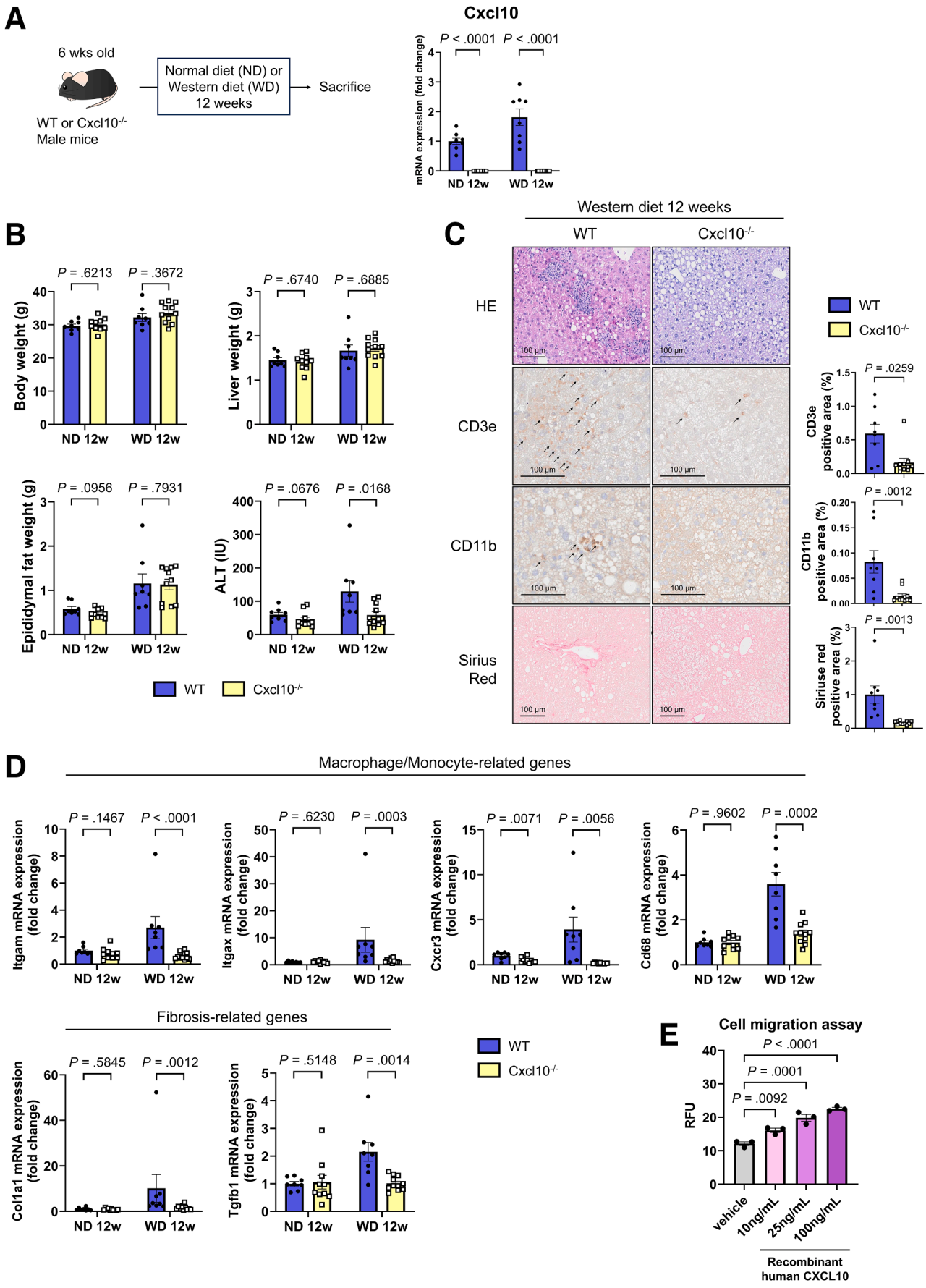
Macrophage-derived IL-1β Induces CCL2 Expression in HSCs via JNK Activation

Finally, based on the spatial transcriptomic findings that HSCs also expressed IL1R1 and exhibited elevated expression of CCL2 transcripts (Figure 10*D*, Figure 12*C*), we evaluated whether macrophage-derived IL-1β could directly induce chemokine production in HSCs. When LX-2 cells were cultured with conditioned medium from ATG7-deficient THP-1 macrophages, *CCL2* expression was markedly increased, accompanied by the activation of JNK and p38 MAPK signaling (Figure 13*A* and *B*). This induction was attenuated by IL1Ra and was significantly suppressed by JNK and p38 MAPK inhibition (Figure 13*C*), indicating that IL1β–IL1R1 signaling drives *CCL2* upregulation in HSCs via MAPK pathways. Furthermore, treatment with recombinant human IL-1β alone increased *CCL2* expression in a dose-dependent manner (Figure 13*D*). These data suggest that macrophage-derived IL-1β not only activates LSECs but also stimulates HSCs to produce CCL2, potentially amplifying immune cell recruitment and fibrotic remodeling in individuals with MASH.

Discussion

In this study, we demonstrated that lipotoxic stress impairs autophagy in macrophages, accompanied by decreased TFEB activity, leading to increased secretion of IL-1β. This macrophage-derived IL-1β induced the expression of *CXCL10* and *CCL2* in LSECs through the activation of JNK and p38 MAPK pathways. In a MASH mouse model, genetic deletion of endothelial Il1r1 and systemic Cxcl10 deficiency ameliorated hepatic inflammation and fibrosis, and pharmacological inhibition of IL1R1 with anakinra produced similar therapeutic benefits. The spatial transcriptomic analysis further revealed that IL1B–IL1R1 signaling was enriched in periportal EC subsets that highly expressed chemokines and were located in close proximity to MoMFs. These findings indicate that macrophage–LSEC communication establishes periportal inflammatory–fibrotic niches that promote immune cell recruitment. In addition to LSECs, HSCs also responded to IL-1β by upregulating *CCL2*, suggesting that macrophage-derived IL-1β amplifies chemokine signaling through multiple NPC types.

Figure 6. (***See previous page***). **EC-specific Il1r1 KO improves MASH pathology progression induced by a WD.** (*A*) Phenotype and WD intake of $Il1r1^{flox/flox}$ or $Il1r1^{\Delta EC}$ mice (n = 9–11/group). (*B*) Histological evaluation of liver tissues in the WD group (n = 11/group). (*C*) Inflammation and fibrosis-related gene expression in liver tissues (n = 9–11/group). (*D*) Gene expression in isolated LSECs after 16 weeks of WD feeding (n = 10/group).


A
6 wks old
WT or Cxcl10-/-
Male mice
Normal diet (ND) or
Western diet (WD)
12 weeks
Sacrifice
Cxcl10
P < .0001 P < .0001
mRNA expression (fold change)
ND 12w
WD 12w
B
P = .6213 P = .3672
Body weight (g)
P = .6740 P = .6885
Liver weight (g)
P = .0956 P = .7931
Epididymal fat weight (g)
P = .0676 P = .0168
ALT (IU)
WT
Cxcl10-/-
C
Western diet 12 weeks
WT
Cxcl10-/-
HE
CD3e
CD11b
Sirius Red
100 μm
P = .0259
CD3e positive area (%)
P = .0012
CD11b positive area (%)
P = .0013
Siriuse red positive area (%)
D
Macrophage/Monocyte-related genes
P = .1467 P < .0001
Itgam mRNA expression (fold change)
P = .6230 P = .0003
Itgax mRNA expression (fold change)
P = .0071 P = .0056
Cxcr3 mRNA expression (fold change)
P = .9602 P = .0002
Cd68 mRNA expression (fold change)
Fibrosis-related genes
P = .5845 P = .0012
Col1a1 mRNA expression (fold change)
P = .5148 P = .0014
Tgfb1 mRNA expression (fold change)
E
Cell migration assay
P < .0001
P = .0001
P = .0092
RFU
vehicle
10ng/mL
25ng/mL
100ng/mL
Recombinant human CXCL10

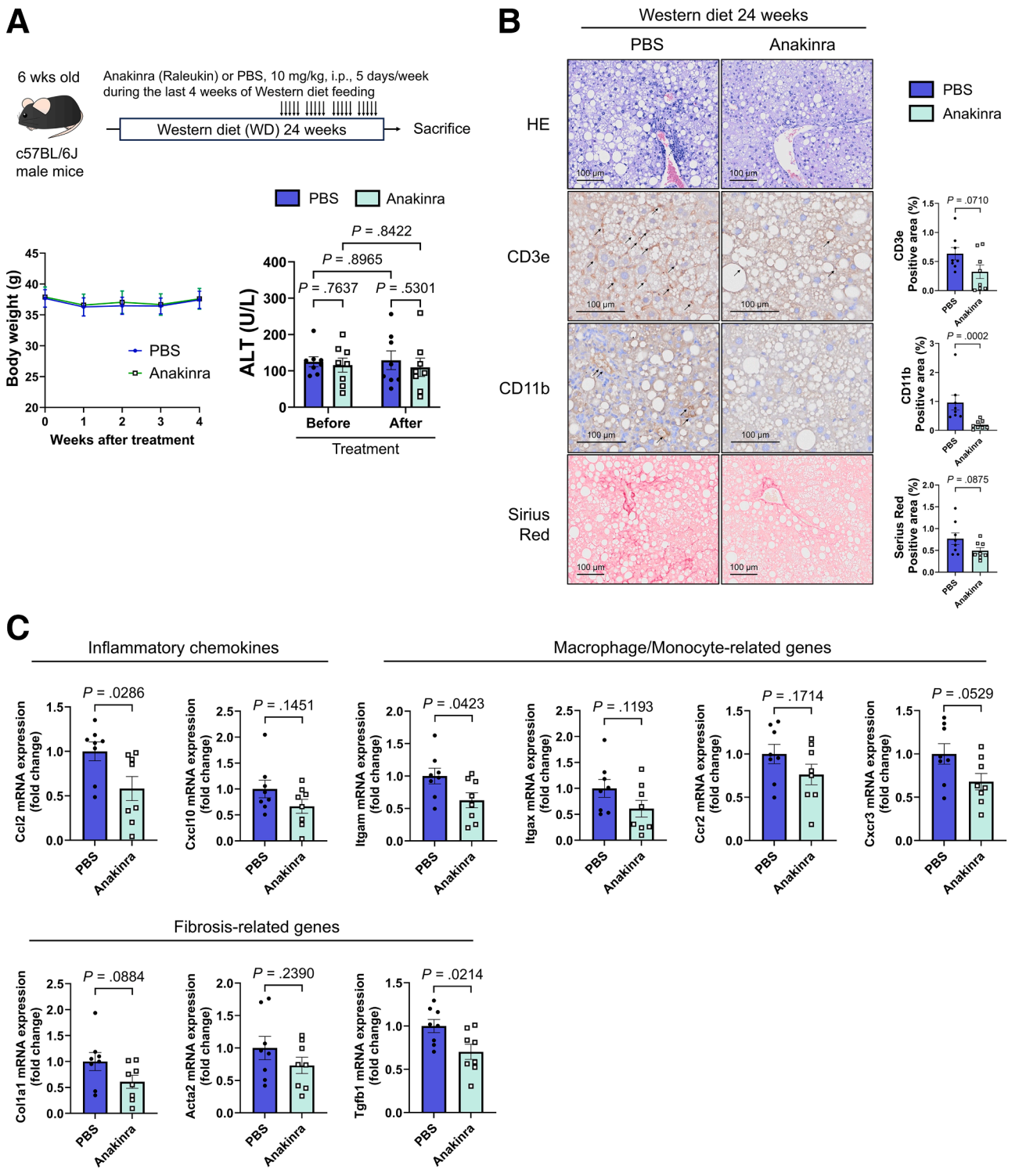
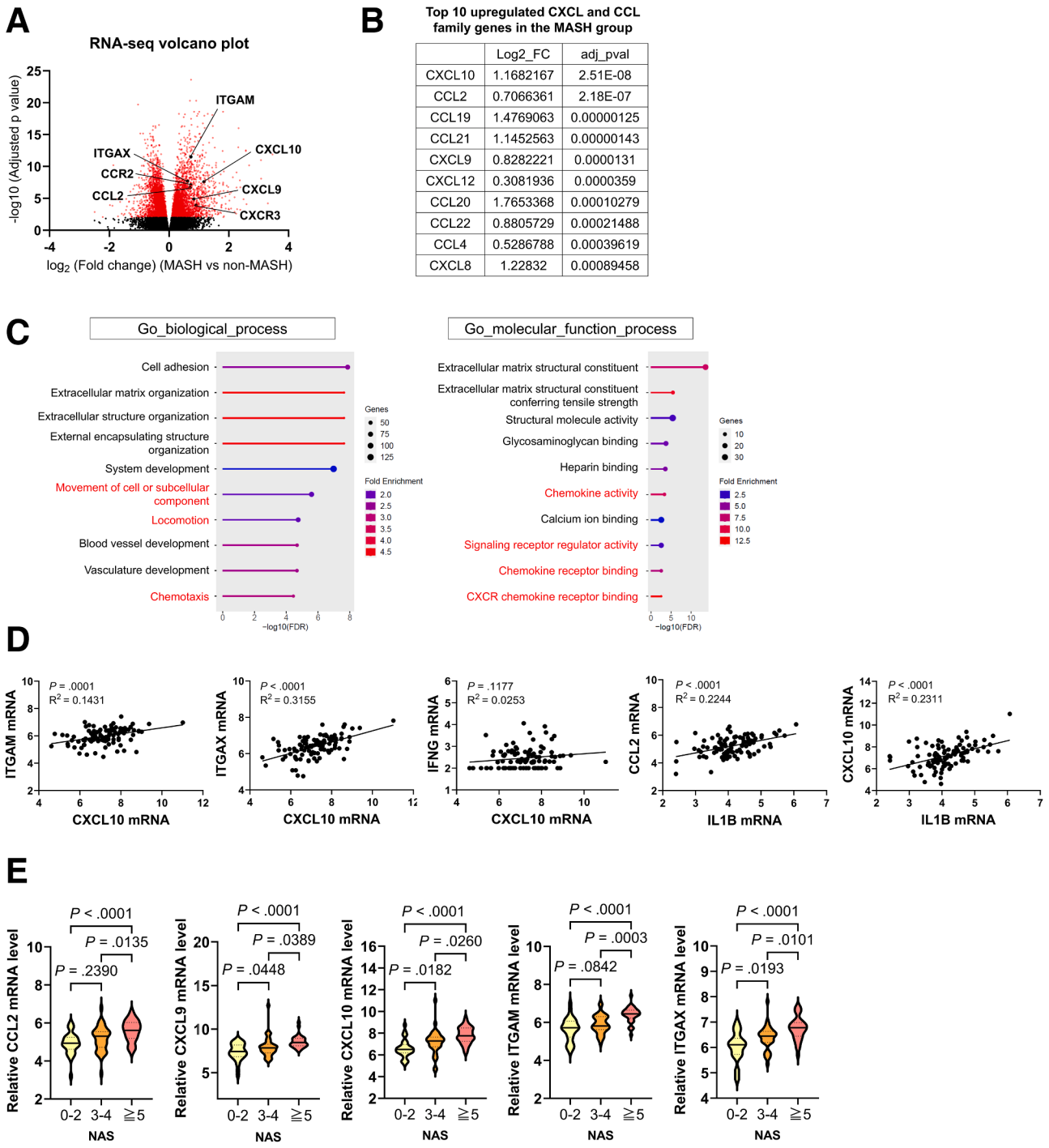


Figure 8. Anakinra exerts potential therapeutic effects on a MASH mouse model. (*A*) Therapeutic schedule of anakinra treatment in the MASH mouse model and changes in body weight and serum ALT levels before and after treatment. (*B*) Histological evaluation of liver tissues (n = 8 mice/group). (*C*) Inflammation and fibrosis-related gene expression in liver tissues (n = 8 mice/group).

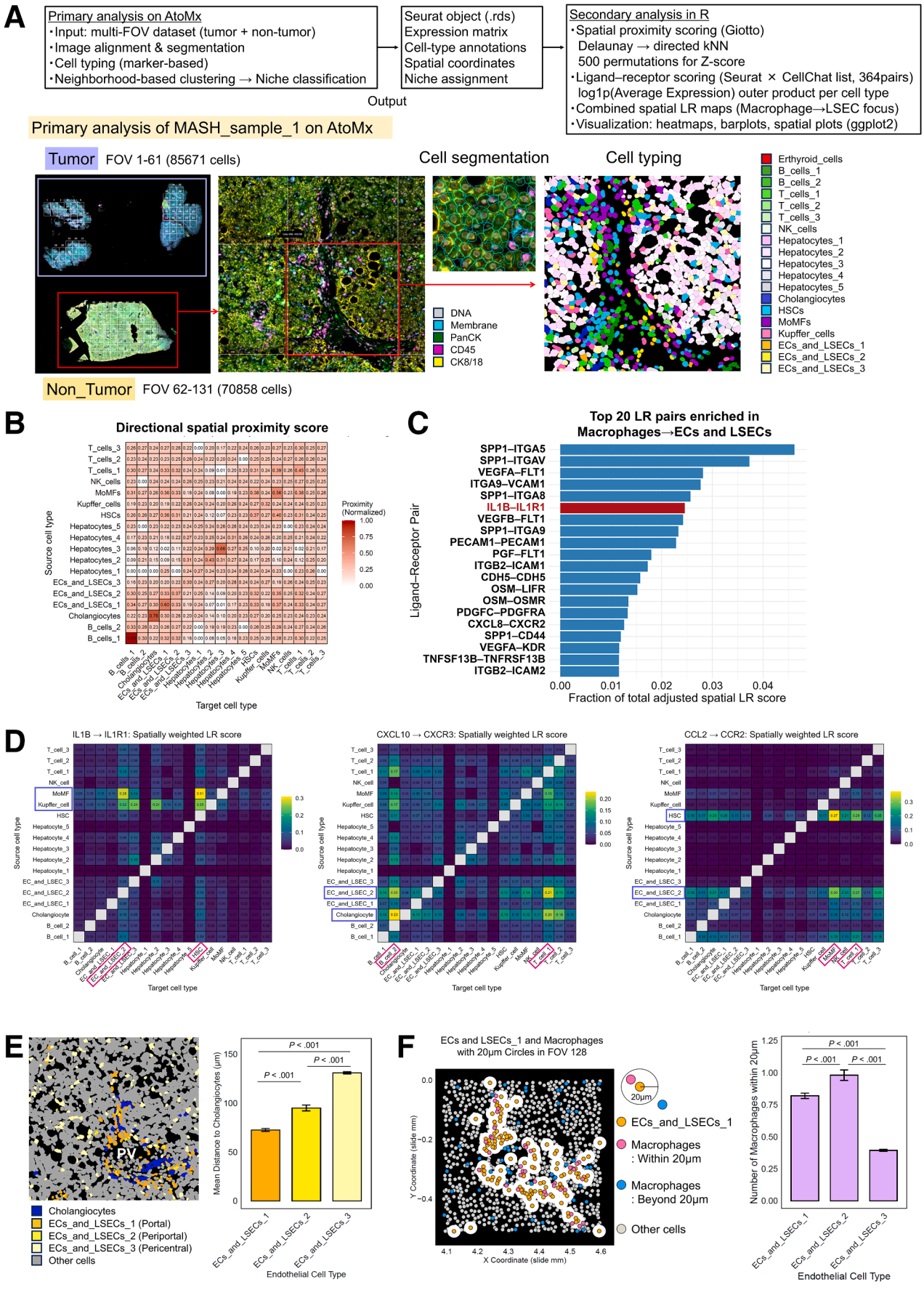
Figure 7. (***See previous page***). **Systemic Cxcl10 KO improves MASH pathology progression induced by a WD.** (*A*) Cxcl10 gene expression in liver tissues (n = 8–11/group). (*B*) Phenotype of WT or Cxcl10$^{-/-}$ mice (n = 8–11/group). (*C*) Histological evaluation of liver tissue in the WD group (n = 8–11/group). (*D*) Macrophage/monocyte and fibrosis-related gene expression in liver tissues (n = 8–11/group). (*E*) A cell migration assay was performed on THP-1 cells using a CytoSelect 24-well cell migration assay (catalog number 093-05991; FUJIFILM Wako Pure Chemical Corporation). THP-1 cells were placed in the upper chamber, and after adding human recombinant CXCL10 at various concentrations, the cells were incubated for 24 hours. The cells that migrated to the lower chamber were dissolved with a specified reagent, and absorbance was measured (n = 3/group). RFU, relative fluorescence unit.



	Log2_FC	adj_pval
CXCL10	1.1682167	2.51E-08
CCL2	0.7066361	2.18E-07
CCL19	1.4769063	0.00000125
CCL21	1.1452563	0.00000143
CXCL9	0.8282221	0.0000131
CXCL12	0.3081936	0.0000359
CCL20	1.7653368	0.00010279
CCL22	0.8805729	0.00021488
CCL4	0.5286788	0.00039619
CXCL8	1.22832	0.00089458

Figure 9. Macrophage-LSEC-mediated CXCL10 induction is involved in the progression of human MASH pathology. (*A–E*) RNA-seq analysis of 98 patients with MASLD (GSE167523). (*A*) Volcano plot and enrichment analysis of differentially expressed genes (DEGs) based on RNA-seq. (*B*) Top 10 upregulated CXCL and CCL family genes in the MASH group compared with the non-MASH group, ranked by *P* value. (*C*) DEG enrichment analysis plots using Gene Ontology (GO) biological process (*left*) and GO molecular function process (*right*). The pathway names related to chemokines and cell migration are highlighted in *red*. (*D*) Correlation plot of inflammation-related gene expression levels. (*E*) Expression of inflammation-related genes by NAFLD Activity Score. The *solid line* in the plot represents the median, and the *dashed lines* indicate the quartiles.

With respect to the role of LSECs in liver disease, previous studies have focused primarily on adhesion molecules such as ICAM-1 and E-selectin, with few reports on chemokine release by LSECs themselves.[21,22] In this study, we detected increased CXCL10 and CCL2 expression in LSECs during MASH. RNA sequencing (RNA-seq) of existing


A
Primary analysis on AtoMx
・Input: multi-FOV dataset (tumor + non-tumor)
・Image alignment & segmentation
・Cell typing (marker-based)
・Neighborhood-based clustering → Niche classification
Seurat object (.rds)
Expression matrix
Cell-type annotations
Spatial coordinates
Niche assignment
Output
Secondary analysis in R
・Spatial proximity scoring (Giotto)
Delaunay → directed kNN
500 permutations for Z-score
・Ligand–receptor scoring (Seurat × CellChat list, 364pairs)
log1p(Average Expression) outer product per cell type
・Combined spatial LR maps (Macrophage→LSEC focus)
・Visualization: heatmaps, barplots, spatial plots (ggplot2)
Primary analysis of MASH_sample_1 on AtoMx
Tumor FOV 1-61 (85671 cells)
Cell segmentation
Cell typing
DNA
Membrane
PanCK
CD45
CK8/18
Erthyroid_cells
B_cells_1
B_cells_2
T_cells_1
T_cells_2
T_cells_3
NK_cells
Hepatocytes_1
Hepatocytes_2
Hepatocytes_3
Hepatocytes_4
Hepatocytes_5
Cholangiocytes
HSCs
MoMFs
Kupffer_cells
ECs_and_LSECs_1
ECs_and_LSECs_2
ECs_and_LSECs_3
Non_Tumor FOV 62-131 (70858 cells)
B
Directional spatial proximity score
Source cell type
Target cell type
Proximity (Normalized)
C
Top 20 LR pairs enriched in Macrophages→ECs and LSECs
Ligand–Receptor Pair
SPP1–ITGA5
SPP1–ITGAV
VEGFA–FLT1
ITGA9–VCAM1
SPP1–ITGA8
IL1B–IL1R1
VEGFB–FLT1
SPP1–ITGA9
PECAM1–PECAM1
PGF–FLT1
ITGB2–ICAM1
CDH5–CDH5
OSM–LIFR
OSM–OSMR
PDGFC–PDGFRA
CXCL8–CXCR2
SPP1–CD44
VEGFA–KDR
TNFSF13B–TNFRSF13B
ITGB2–ICAM2
Fraction of total adjusted spatial LR score
D
IL1B → IL1R1: Spatially weighted LR score
CXCL10 → CXCR3: Spatially weighted LR score
CCL2 → CCR2: Spatially weighted LR score
Source cell type
Target cell type
E
PV
Cholangiocytes
ECs_and_LSECs_1 (Portal)
ECs_and_LSECs_2 (Periportal)
ECs_and_LSECs_3 (Pericentral)
Other cells
Mean Distance to Cholangiocytes (μm)
P < .001
Endothelial Cell Type
F
ECs and LSECs_1 and Macrophages with 20μm Circles in FOV 128
Y Coordinate (slide mm)
X Coordinate (slide mm)
20μm
ECs_and_LSECs_1
Macrophages : Within 20μm
Macrophages : Beyond 20μm
Other cells
Number of Macrophages within 20μm
P < .001
Endothelial Cell Type

liver biopsy samples confirmed that the expression of these genes increased with MASH progression. Furthermore, we detected high *IL1R1* gene expression in ECs and HSCs in both mice and humans. Although CXCL10 expression is primarily induced by interferon (IFN)-γ stimulation and signals through the CXCR3 receptor, its expression showed little correlation with IFN-γ but was highly correlated with IL1B in liver biopsy samples from patients with MASLD (Figure 9*D*). *CXCL10* expression in the liver has been reported to play a role in monocyte and macrophage recruitment and MASH pathogenesis, but research on the role of LSEC-derived CXCL10 in MASH is limited. In our study, EC-specific IL1R1-KO mice with MASH presented reduced inflammatory cell infiltration due to suppressed chemokine expression in LSECs, which also led to decreased liver fibrosis. Although previous studies have demonstrated that hepatocyte-specific IL1R1 knockout improved MASH pathology,[23] our study is the first to demonstrate the role of IL1R1 in ECs during MASH.

Studies using liver tissues from patients with MASLD/MASH have shown that CXCL10 and CCL2 expression correlate strongly with disease progression. Given that the IL-1β–IL-1R1 axis plays a crucial role in the expression of these genes, IL-1R1 inhibitors may be useful in suppressing MASH progression. The potential of targeting IL-1 for the treatment of liver diseases has previously been discussed.[24,25] Anakinra, an IL-1R1 inhibitor, is a United States Food and Drug Administration (FDA)-approved treatment for conditions such as rheumatoid arthritis and Still's disease. A multicenter, randomized, double-blind, placebo-controlled trial (the DASH trial) is currently evaluating the efficacy of anakinra for alcoholic steatohepatitis treatment.[26] Anakinra has also been reported to improve insulin sensitivity and glucose tolerance in diabetic patients,[27,28] raising prospects for its future application in MASLD, which is strongly associated with glucose intolerance. In our MASH mouse model, short-term administration of anakinra led to reduced hepatic inflammation and a trend toward attenuated fibrosis, accompanied by decreased expression of Ccl2, Itgam, and Tgfb1 in the liver tissue and reduced $CD11b^{+}$ immune cell infiltration. These findings provide in vivo support that pharmacological IL-1R1 blockade can mitigate chemokine-mediated inflammatory responses and may help attenuate inflammatory–fibrotic progression in patients with MASH.

Evaluating autophagy in vivo is challenging, and there has been debate over whether autophagy is activated or suppressed in liver tissues from patients with MASH. We previously reported that fatty acid stimulation disrupts the late stages of autophagy in hepatocytes.[16] In this study, we focused on TFEB, a key regulator of lysosomal biogenesis, during the late stages of autophagy. We observed a reduction in TFEB expression and autophagy suppression in THP-1 macrophages subjected to fatty acid overload. TFEB translocates to the nucleus in response to lysosomal stress, contributing to the maintenance of lysosomal function. However, the accumulation of chronic stress may lead to a reduction in TFEB activity over time, resulting in lysosomal dysfunction. This suggests a dual mechanism in which the nuclear translocation of TFEB serves as an initial adaptive response, whereas its subsequent downregulation contributes to chronic disease progression. Autophagy impairment associated with TFEB downregulation has also been reported in ethanol-induced liver injury, highlighting the importance of improving lysosomal function to slow the progression of steatohepatitis.[29] Ezetimibe and curcumin have been reported to improve autophagy as TFEB activators,[30–32] and the development of TFEB activators or autophagy-targeted therapies for the treatment of fatty liver diseases, including MASH, is anticipated in the future.

In conclusion, impaired autophagy in hepatic macrophages leads to increased IL-1β secretion, which activates periportal LSECs via IL1R1 signaling to induce the production of chemokines that recruit immune cells and amplify inflammatory–fibrotic remodeling in individuals with MASH. These results identify macrophage autophagy and IL-1β–IL1R1 signaling as actionable therapeutic targets that warrant further investigation in the treatment of MASH.

Materials and Methods

Mice

B6.129P2-Lyzs<tm1(cre)Ifo> mice (RBRC02302) (LysM-Cre mice) were provided by the RIKEN BRC through the National Bio-Resource Project of the MEXT, Japan. The $Atg7^{flox/flox}$ mice were kindly provided by Professor Masaaki Komatsu of Juntendo University.[33] These mice were crossed to produce LysM-Cre $Atg7^{flox/flox}$ ($Atg7^{\Delta Mye}$) mice.

$Cdh5\text{-}Cre^{ERT2}$ mice were generously provided by Professor Yoshiaki Kubota in the Department of Anatomy at Keio University School of Medicine.[34] B6.129(Cg)-$Il1r1^{<tm1.1Rbl>}$/J (#028398) ($Il1r1^{flox/flox}$) mice were purchased from Jackson Laboratory and crossed with $Cdh5\text{-}Cre^{ERT2}$ mice to produce $Cdh5\text{-}Cre^{ERT2}$ $Il1r1^{flox/flox}$ ($Il1r1^{\Delta EC}$) mice. Tamoxifen (100 mg/kg/day; intraperitoneally) was administered once daily for 5 consecutive days to mice at 4 to 5 weeks of age to induce

Figure 10. (*See previous page*). **Spatial transcriptomic analysis reveals a dominant IL1B–IL1R1 axis between macrophages and LSECs, with increased chemokine expression in periportal ECs accompanied by increased macrophage proximity.** (*A*) Workflow for the analysis of liver tissues from a patient with MASH (CosMx_MASH_sample_1) using CosMx. (*B*) Heatmap of the directional spatial proximity score across source-target cell type pairs. (*C*) Top 20 LR pairs enriched in macrophage → endothelial cell/LSEC interactions based on spatial LR scores. (*D*) Heatmaps of spatially weighted LR scores. From left to right: IL1B–IL1R1, CXCL10–CXCR3, and CCL2–CCR2. Higher values indicate the preferential enrichment of source→target interactions. (*E*) (*Left panel*) Positional relationship between each EC and cholangiocyte in the FOV. (*Right panel*) Comparison of the shortest distance from each EC to the nearest cholangiocyte. (*F*) (*Left panel*) Positional relationship between ECs and LSECs and macrophages in the FOV. The *white circles* represent a 20-μm radius from each EC. (*Right panel*) Comparison of the average number of macrophages within 20 μm of each EC.

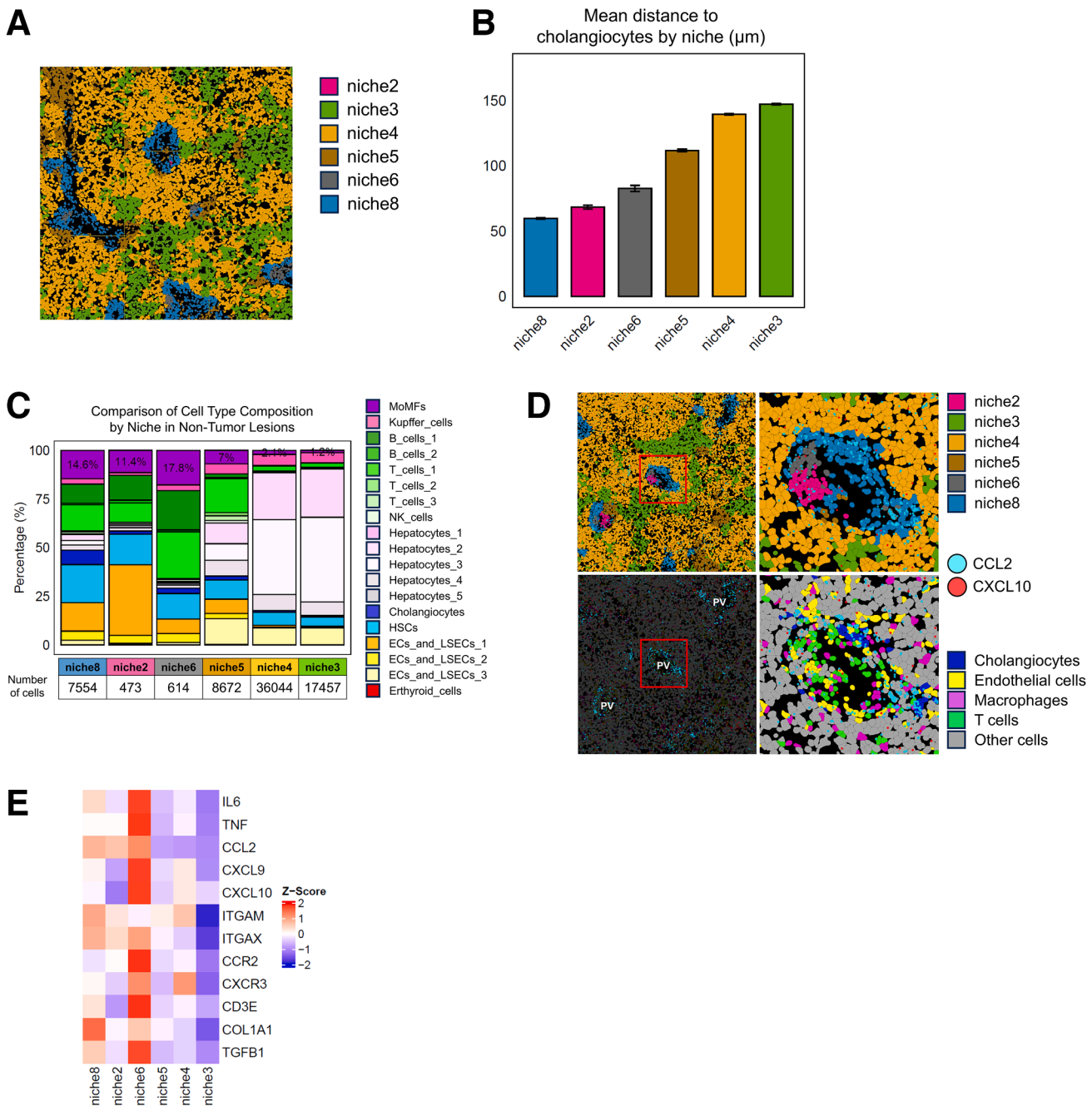
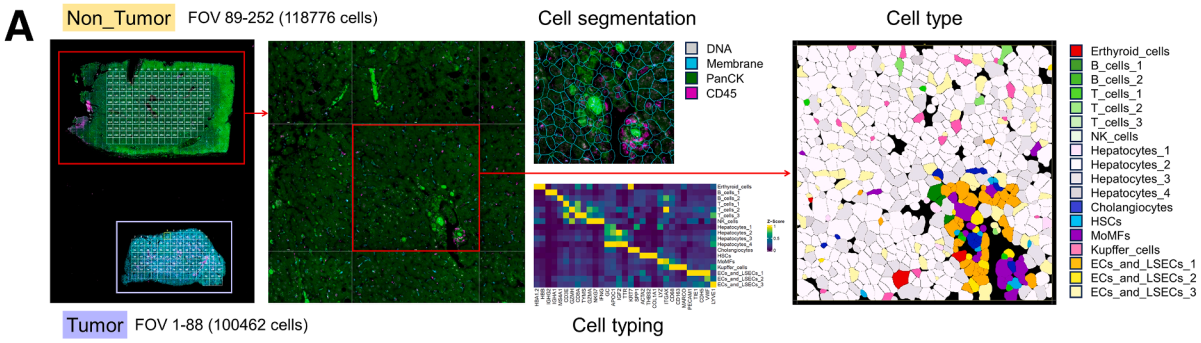
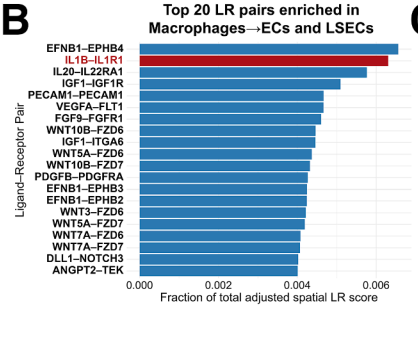


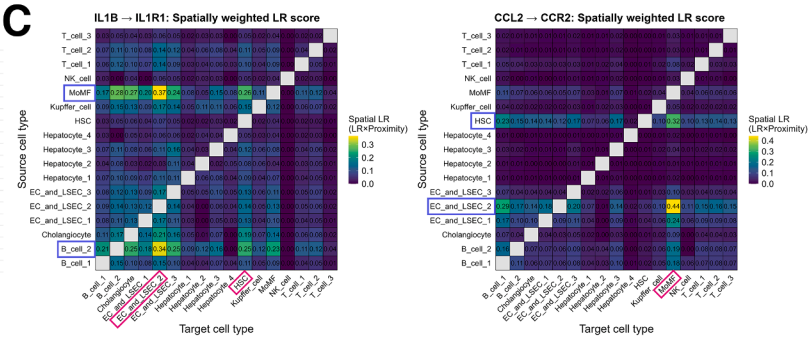
Figure 11. Periportal niches enriched for inflammation and fibrosis in MASH liver tissue. (*A*) Image of the FOV with the non-tumor regions color-coded by niche. (*B*) Bar plot of the mean distance to cholangiocytes by niche. (*C*) Bar plot showing the proportions of cell types in each niche of the non-tumor region. (*D*) Images of the FOV color-coded by niche (*upper panel*) or cell type (*lower panel*), merged with a plot of the expression of the CCL2 and CXCL10 transcripts. ECs are a combination of ECs and LSECs 1, 2, and 3; Macrophages are a combination of KCs and MoMFs; and T-cells are a combination of T cells 1, 2, and 3. (*E*) Heatmap of inflammation- and fibrosis-related gene expression across each niche.

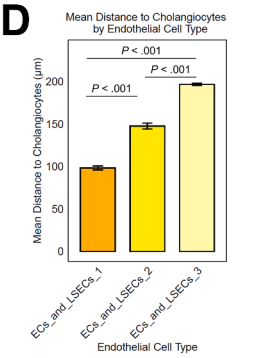
EC-specific deletion. B6.129S4-Cxcl10^{tm1Adl}/J (#006087) (Cxcl10$^{-/-}$) mice were purchased from Jackson Laboratory. All these genetically modified mice were backcrossed with C57BL/6J mice for more than 10 generations. As a control for Cxcl10$^{-/-}$ mice, 4-week-old C57BL6/J mice were purchased from Jackson Laboratory Japan and were co-housed with Cxcl10$^{-/-}$ mice.

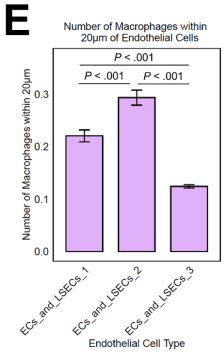
The mice were fed either an ND (CRF-1; Oriental Yeast Company) or a WD for 12 to 48 weeks. The WD (D20092804) was custom-formulated by Research Diets, Inc to be high in fat (36.4% kcal, primarily from milk fat), cholesterol (1.21%), and sucrose-enriched carbohydrates (48.4% kcal).

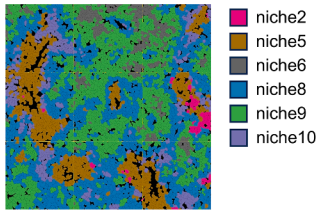

A
Non_Tumor
FOV 89-252 (118776 cells)
Cell segmentation
Cell type
DNA
Membrane
PanCK
CD45
Erythroid_cells
B_cells_1
B_cells_2
T_cells_1
T_cells_2
T_cells_3
NK_cells
Hepatocytes_1
Hepatocytes_2
Hepatocytes_3
Hepatocytes_4
Cholangiocytes
HSCs
MoMFs
Kupffer_cells
ECs_and_LSECs_1
ECs_and_LSECs_2
ECs_and_LSECs_3
Tumor
FOV 1-88 (100462 cells)
Cell typing

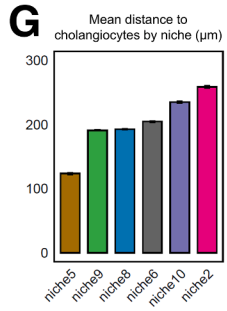

B
Top 20 LR pairs enriched in Macrophages→ECs and LSECs
Ligand–Receptor Pair
EFNB1–EPHB4
IL1B–IL1R1
IL20–IL22RA1
IGF1–IGF1R
PECAM1–PECAM1
VEGFA–FLT1
FGF9–FGFR1
WNT10B–FZD6
IGF1–ITGA6
WNT5A–FZD6
WNT10B–FZD7
PDGFB–PDGFRA
EFNB1–EPHB3
EFNB1–EPHB2
WNT3–FZD6
WNT5A–FZD7
WNT7A–FZD6
WNT7A–FZD7
DLL1–NOTCH3
ANGPT2–TEK
0.000
0.002
0.004
0.006
Fraction of total adjusted spatial LR score

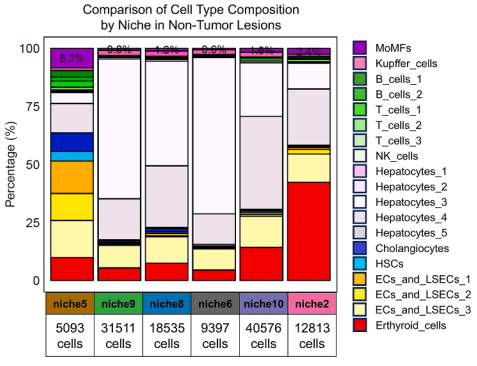

C
IL1B → IL1R1: Spatially weighted LR score
CCL2 → CCR2: Spatially weighted LR score
Source cell type
Target cell type
Spatial LR (LR×Proximity)

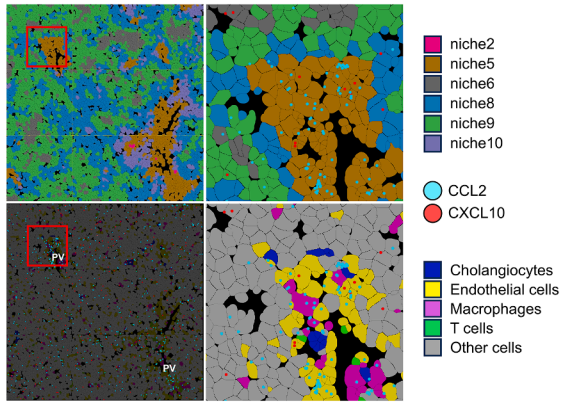

D
Mean Distance to Cholangiocytes by Endothelial Cell Type
Mean Distance to Cholangiocytes (μm)
P < .001
ECs_and_LSECs_1
ECs_and_LSECs_2
ECs_and_LSECs_3
Endothelial Cell Type

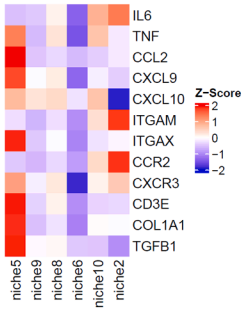

E
Number of Macrophages within 20μm of Endothelial Cells
Number of Macrophages within 20μm
P < .001
ECs_and_LSECs_1
ECs_and_LSECs_2
ECs_and_LSECs_3
Endothelial Cell Type


F
niche2
niche5
niche6
niche8
niche9
niche10


G
Mean distance to cholangiocytes by niche (μm)
niche5
niche9
niche8
niche6
niche10
niche2


H
Comparison of Cell Type Composition by Niche in Non-Tumor Lesions
Percentage (%)
8.3%
0.8%
1.8%
0.6%
1.8%
24.3%
niche5
niche9
niche8
niche6
niche10
niche2
5093 cells
31511 cells
18535 cells
9397 cells
40576 cells
12813 cells
MoMFs
Kupffer_cells
B_cells_1
B_cells_2
T_cells_1
T_cells_2
T_cells_3
NK_cells
Hepatocytes_1
Hepatocytes_2
Hepatocytes_3
Hepatocytes_4
Hepatocytes_5
Cholangiocytes
HSCs
ECs_and_LSECs_1
ECs_and_LSECs_2
ECs_and_LSECs_3
Erythroid_cells


I
PV
niche2
niche5
niche6
niche8
niche9
niche10
CCL2
CXCL10
Cholangiocytes
Endothelial cells
Macrophages
T cells
Other cells


J
IL6
TNF
CCL2
CXCL9
CXCL10
ITGAM
ITGAX
CCR2
CXCR3
CD3E
COL1A1
TGFB1
Z-Score
niche5
niche9
niche8
niche6
niche10
niche2

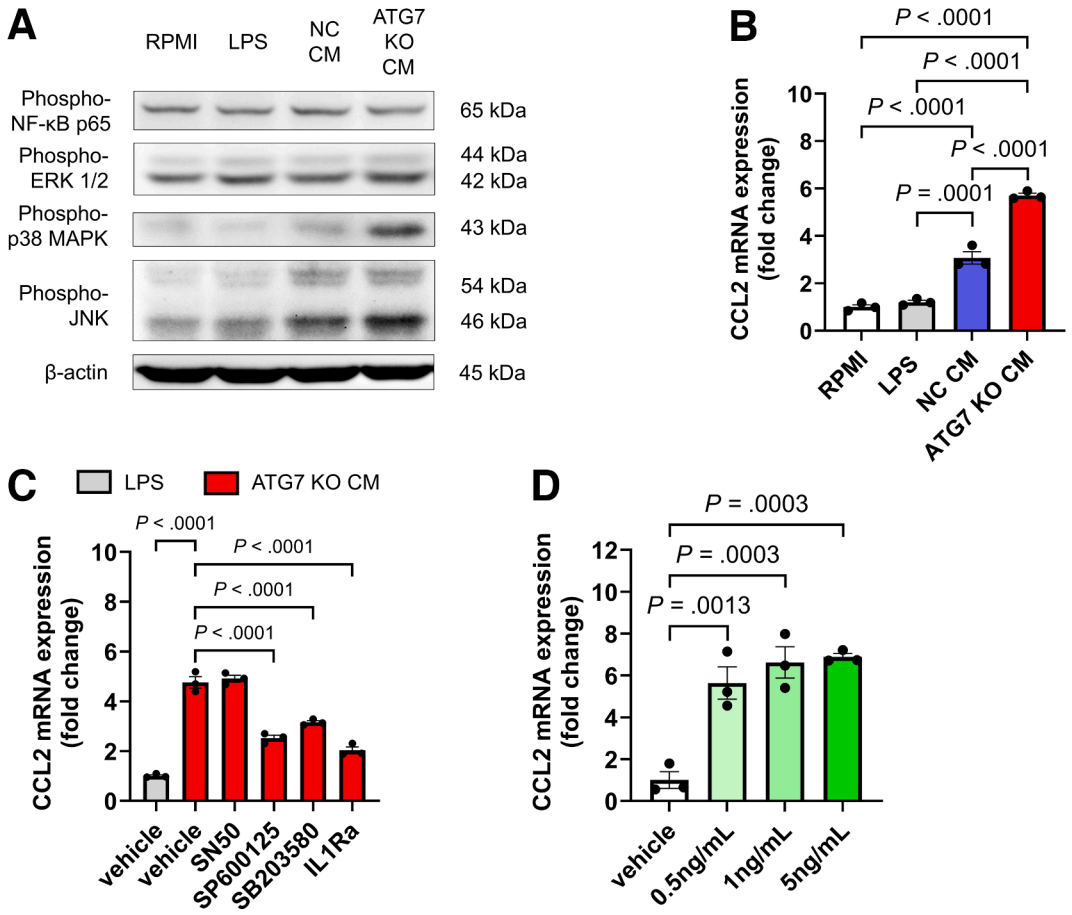


Figure 13. Macrophage-derived IL-1β increases CCL2 expression in HSCs via JNK activation. (*A*) Evaluation of the levels of NF-κB or MAPK-related proteins in LX-2 cells. (*B, C*) CCL2 gene expression in LX-2 cells treated with the control medium or THP-1 macrophage conditioned medium (n = 3/group). SN50, NF-κB inhibitor; SP600125, JNK inhibitor; SB203580, p38 MAPK inhibitor. (*D*) Evaluation of CCL2 expression in TMNK-1 cells after 48 hours of stimulation with recombinant human IL-1β (5 ng/mL) in the presence of SP600125 and SB203580 (n = 4/group).

We performed an experiment using the pharmacological inhibitor anakinra (Raleukin; Synonyms: Kineret; Anakinra; HY-108841; MedChemExpress) to evaluate the therapeutic effect of IL1R1 signaling on MASH progression. Mice were fed a WD for 24 weeks and were administered either phosphate buffered saline (PBS) or anakinra (10 mg/kg, intraperitoneally, 5 days per week) during the final 4 weeks. Body weight and serum ALT levels were measured prior to treatment initiation to ensure comparable baseline conditions between groups.

Glucose Tolerance Test

The ND group and the WD group were fasted overnight before glucose tolerance testing (GTT). At 9:00 the next morning, a glucose solution (D-(+)-Glucose, D-G8270; Sigma-Aldrich) at a dosage of 1 g/kg body weight was injected intraperitoneally.[13] Blood samples were collected from the tail vein at designated time points, and blood glucose levels were measured.

Collection of Mouse Hepatocytes, Liver Macrophages, and LSECs

As we previously reported,[35] the pronase–collagenase perfusion procedure was used to dissociate hepatocytes and NPCs into single-cell suspensions. The collected cells were suspended in Roswell Park Memorial Institute (RPMI)

Figure 12. (*See previous page*). Spatial transcriptomic validation of periportal inflammatory–fibrotic niches and macrophage–LSEC IL1B–IL1R1 interactions in a sample from an independent patient with MASH. (*A*) Workflow for the analysis of liver tissues from a patient with MASH (CosMx_MASH_sample_2) using CosMx. (*B*) Top 20 LR pairs enriched in macrophage → EC/LSEC interactions based on spatial LR scores. (*C*) Heatmaps of spatially weighted LR scores. (*D*) Comparison of the shortest distance from each EC to the nearest cholangiocyte. (*E*) Comparison of the average number of macrophages within 20 μm of each EC. (*F*) Image of the FOV with the non-tumor regions color-coded by niche. (*G*) Bar plot of the mean distance to cholangiocytes by niche. (*H*) Bar plot showing the proportions of cell types in each niche of the non-tumor region. (*I*) Images of the FOV color-coded by niche (*upper panel*) or cell type (*lower panel*), merged with a plot of the expression of the CCL2 and CXCL10 transcripts. (*J*) A heatmap of inflammation- and fibrosis-related gene expression across each niche.

medium containing 2% FBS, filtered through a 70-μm mesh filter, and centrifuged at 500 $\times$ g for 10 minutes. After the supernatant was discarded, the pellet was resuspended, and the process was repeated. The pellet was then resuspended in RPMI medium and centrifuged at 50 $\times$ g for 10 minutes to separate the supernatant, which contained the NPCs, from the pellet containing hepatocytes. This separation process was repeated 2 to 4 times to increase the purity. Finally, the NPCs were collected from the pellet after centrifugation at 500 $\times$ g for 10 minutes. From the collected NPCs, LSECs were isolated using anti-CD146 MACS beads (130-092-007; Miltenyi Biotec), followed by isolation of liver macrophages using anti-F4/80 MACS beads (130-110-443; Miltenyi Biotec).[36]

Flow Cytometry

After pronase and collagenase perfusion, NPCs isolated from mouse liver tissues were stained using the following antibodies: anti-CD45 (553080; BD Pharmingen), anti-Ly-6C (560593; BD Pharmingen), anti-Ly-6G (746448; BD Pharmingen), anti-CD11b (561689; BD Pharmingen), anti-F4/80 (565411; BD Pharmingen), and anti-7-AAD (559925; BD Pharmingen). The cells were then processed using a BD Cytofix/Cytoperm Fixation/Permeabilization Kit (554714; BD Biosciences) and stored at -80 °C. The frozen cells were thawed and stained for intracellular p62 expression with an anti-SQSTM1/p62 antibody [EPR4844] (ab109012; Abcam) and pre-adsorbed goat anti-rabbit IgG H&L (Alexa Fluor 647) (ab150083; Abcam). The stained cells were analyzed using a BD FACSCanto II Clinical Flow Cytometry System (BD Biosciences) and processed with FlowJo v10 software (BD Biosciences). Among the $CD45^{+}Ly6G^{-}$ cells, those characterized as $CD11b^{high}$ $F4/80^{int}$ were classified as MoMFs, and those characterized as $CD11b^{int}$ $F4/80^{high}$ were classified as KCs. The mean fluorescence intensity of p62 was measured for both cell types. The mice used in the study were $Atg7^{flox/flox}$ mice, which served as wild-type controls.

We quantified the absolute number of hepatic MoMFs by calculating cell counts based on the total yield of isolated NPCs and flow cytometric frequencies using the following formula:

Number of isolated MoMFs = Total live NPCs $\times$ (%$CD45^{+}$ of live) $\times$ (%MoMF of $CD45^{+}$).

Single-cell RNA-seq Analysis

The mouse livers were perfused with pronase and collagenase, followed by centrifugation at 50 $\times$ g for 10 minutes to separate hepatocytes and NPCs. The cells were mixed at a ratio of approximately 1:4 (hepatocytes to NPCs) to improve the analysis quality to focus on the function of NPCs. Single-cell analysis was performed using a BD Rhapsody Express System (BD Biosciences) according to the manufacturer's protocol. Rhapsody WTA libraries were sequenced on a DNBSEQ-G400RS (MGIF-400; MGI Tech Co, Ltd), and raw sequence reads were demultiplexed to generate fastq files for each sample using SplitBarcode v2.0.0 (MGI Tech Co, Ltd). Single-cell RNA data were analyzed using Seurat (version 5) in R (version 4.3.3).

Histological Analysis

Paraffin-embedded sections of mouse liver fixed in 10% formalin were prepared and stained with hematoxylin and eosin (H&E) and Sirius Red. Sirius Red staining was performed using a Picrosirius Red Staining Kit (24901; Polysciences, Inc). To evaluate inflammatory cell infiltration, we used a VECTASTAIN ABC-HRP Kit and peroxidase (rat immunoglobulin G) (PK-4004; Vector Laboratories) and stained the samples with a rabbit anti-CD3 epsilon antibody (ab5690; Abcam) and a rabbit anti-CD11b antibody [EPR1344] (ab133357; Abcam). The stained sections were imaged using a VS200 Research Slide Scanner (EVIDENT), and positive areas were quantified using HALO software (Indica Labs).

Cell Culture

THP-1 cells (JCRB0112), TMNK-1 cells (JCRB1564), and LX-2 cells (JCRB1569) were purchased from the JCRB Cell Bank. TMNK-1 cells and LX-2 cells were cultured in Dulbecco's modified Eagle's medium (DMEM) (D6429; Sigma-Aldrich) supplemented with 10% FBS (16000044; Thermo Fisher Scientific) and 1% antibiotics (15240062; Thermo Fisher Scientific). THP-1 cells were cultured in RPMI medium (R8758; Sigma-Aldrich) supplemented with the same supplements at 37°C and 5% CO_2. THP-1 cells were stimulated with 100 ng/mL phorbol 12-myristate 13-acetate (PMA) (P1585; Sigma-Aldrich) for 48 hours to induce their differentiation into macrophages.[37] After differentiation, the cells were washed 3 times with PBS, fresh RPMI medium was added, and the cells were incubated overnight before being used in subsequent experiments.

Plasmids

Using lentiCRISPR v2-Blast (Addgene, 83480) as a template, we constructed a lentiCRISPR ATG7 KO plasmid and a lentiCRISPR negative control (NC) plasmid using the CRISPR–Cas9 system. The guide RNA sequences for ATG7 were as follows: forward, 5′-CACCGAGAAGAAGCTGAACGAGTAT-3′; reverse, 5′-AAACATACTCGTTCAGCTTCTTCTC-3′. The guide RNA sequences for the negative control were as follows: forward, 5′-CACCGTGGCGGCCCAAACTTAACAC-3′; reverse, 5′-AAACGTGTTAAGTTTGGGCCGCCAC-3′. The constructed plasmids were cotransfected with the PAX2 plasmid (Addgene, #12260) and the VSVG plasmid (Addgene, #8454) into HEK293 cells to generate lentiviruses. The culture supernatant containing the lentiviruses was then applied to THP-1 cells, followed by selection with blasticidin (Sigma–Aldrich, B12150). After selection, single-cell clones were generated by limiting dilution and cultured. The KO efficiency was confirmed by Western blotting.

Enzyme-linked Immunosorbent Assay

THP-1 macrophages were pretreated for 1 hour with 50 μM Z-YVAD-FMK (S8507; Selleck, Houston, TX) before

stimulation. The cells were subsequently stimulated for 24 hours with 25 ng/mL LPS (L2630; Sigma–Aldrich) in combination with bovine serum albumin (BSA), 400 μM PA, 50 nM BFM, or each agent alone. The culture supernatants were then collected. The contents of IL-1β and caspase-1 in the culture supernatants were measured using a Human IL-1 beta/IL-1F2 DuoSet enzyme-linked immunosorbent assay (ELISA) (DY201-05; R&D Systems) and a Human caspase-1/ICE Quantikine ELISA Kit (DCA100; R&D Systems), respectively.

Western Blotting

The protocols for sample preparation, electrophoresis, transfer, luminescence detection, and imaging of the cell lines or liver tissue were performed as previously described.[38] The list of antibodies used is provided in Table 1. Nuclear proteins were extracted using a Nuclear Extraction Kit (Abcam, ab113474) according to the manufacturer's protocol.

Quantitative Real-time Reverse-transcription Polymerase Chain Reaction

Total RNA was extracted from cells or tissues and reverse transcribed to complementary DNA (cDNA) as previously described.[16] Messenger RNA (mRNA) expression was measured using quantitative real-time reverse-transcription polymerase chain reaction (qRT-PCR) with Thunderbird qPCR Master Mix (Toyobo) and TaqMan probes (Thermo Fisher Scientific). The expression of the target genes was normalized to that of β-actin and expressed as fold changes relative to those of the control group. The probes used are listed in Table 2.

Evaluation of Autophagy

PA was prepared as previously described.[39] THP-1 macrophages were stimulated with various concentrations of PA for 24 hours, followed by a 2-hour treatment with or without 125 nM BFM A1 (BioViotica). Proteins were then collected and analyzed by Western blotting. The

Table 1. List of Antibodies Used for Western Blotting

Purchased from	Cat. No.	Protein	Product name	Dilution	Source
Sigma	A5316	β-Actin	Monoclonal anti-β-actin antibody produced in mouse	1:3000	Mouse
Cell Signaling Technology	#13435	Lamin B1	Lamin B1 (D9V6H) rabbit mAb	1:1000	Rabbit
Cell Signaling Technology	#2631	Atg7	Atg7 antibody	1:1000	Rabbit
Cell Signaling Technology	#5144	SQSTM1/p62	SQSTM1/p62 antibody	1:1000	Rabbit
Cell Signaling Technology	#2775	LC3B	LC3B antibody	1:1000	Rabbit
Cell Signaling Technology	#8242	NF-κB p65	NF-κB p65 (D14E12) XP rabbit mAb	1:1000	Rabbit
Cell Signaling Technology	#3033	Phospho-NF-κB p65	Phospho-NF-κB p65 (Ser536) (93H1) rabbit mAb	1:1000	Rabbit
Cell Signaling Technology	#9252	JNK	SAPK/JNK antibody	1:1000	Rabbit
Cell Signaling Technology	#9251	Phospho-JNK	Phospho-SAPK/JNK (Thr183/Tyr185) antibody	1:1000	Rabbit
Cell Signaling Technology	#9212	p38 MAPK	p38 MAPK antibody	1:1000	Rabbit
Cell Signaling Technology	#4511	Phospho-p38 MAPK	Phospho-p38 MAPK (Thr180/Tyr182) (D3F9) XP rabbit mAb	1:1000	Rabbit
Cell Signaling Technology	#4695	Erk1/2	p44/42 MAPK (Erk1/2) (137F5) rabbit mAb	1:1000	Rabbit
Cell Signaling Technology	#4370	Phospho-Erk1/2	Phospho-p44/42 MAPK (Erk1/2) (Thr202/Tyr204) (D13.14.4E) XP rabbit mAb	1:1000	Rabbit
Cell Signaling Technology	#12242	IL-1β	IL-1β (3A6) mouse mAb	1:1000	Mouse
Cell Signaling Technology	#4240	TFEB	TFEB antibody	1:1000	Rabbit
Cell Signaling Technology	#37681	Phospho-TFEB	Phospho-TFEB (Ser211) (E9S8N) rabbit mAb	1:1000	Rabbit
Cell Signaling Technology	#32361	TFEB	TFEB (D4L2P) rabbit mAb	1:1000	Rabbit

Table 2. List of TaqMan Probes Used for qRT-PCR

Species	Gene	Assay ID	Species	Gene	Assay ID
Mouse	Actb	Mm02619580_g1	Human	ACTB	Hs01060665_g1
	Il1b	Mm00434228_m1		CCL2	Hs00234140_m1
	Ccl2	Mm00441242_m1		CXCL9	Hs00171065_m1
	Cxcl9	Mm00434946_m1		CXCL10	Hs00171042_m1
	Cxcl10	Mm00445235_m1		IL1B	Hs01555410_m1
	Cd68	Mm03047343_m1			
	Ccr2	Mm99999051_gH			
	Itgam	Mm00434455_m1			
	Itgax	Mm00498698_m1			
	Cxcr3	Mm99999054_s1			
	Il1r1	Mm00434235_m1			
	Col1a1	Mm00801666_g1			
	Tgfb1	Mm01178820_m1			
	Alb	Mm00802090_m1			
	Lyve1	Mm00475056_m1			
	Adgre1	Mm00802529_m1			
	Clec4f	Mm00443934_m1			
	Atg7	Mm00512209_m1			
	Sqstm1	Mm00448091_m1			
	Fos	Mm00487425_m1			
	Jun	Mm07296811_s1			

qRT-PCR, quantitative real-time reverse-transcription polymerase chain reaction.

autophagic flux index was calculated as the ratio of the LC3-II protein level in the presence of BFM A1 to the level in its absence.

Conditioned Medium Experiments

Culture supernatants from THP-1 macrophages (negative control or ATG7-KO) stimulated with 25 ng/mL LPS were used as conditioned media. This conditioned medium was then mixed with the supernatant of TMNK-1 cells at a 50% volume ratio. After 24 hours, proteins and RNA were collected for analysis. To investigate the effects on the NF-κB and MAPK pathways, TMNK-1 cells were pretreated with various inhibitors for 1 hour, followed by the addition of culture supernatants from LPS-stimulated ATG7 KO THP-1 macrophages. After 24 hours, RNA was harvested from the cells. The inhibitors used were as follows: the NF-κB inhibitor SN50 (HY-P0151; MedChemExpress), the JNK inhibitor SP600125 (HY-12041; MedChemExpress), the p38 MAPK inhibitor SB 203580 (HY-10256; MedChemExpress), and the IL-1R antagonist (IL-1Ra) (093-05991; FUJIFILM Wako Pure Chemical Corporation). To assess the effects of IL-1β, TMNK-1 cells were treated with 5 ng/mL recombinant human IL-1 beta protein (ab9617; Abcam), and RNA was harvested from the cells.

In parallel, conditioned media from THP-1 macrophages stimulated with 25 ng/mL LPS were also added to LX-2 cells at a 50% volume ratio. After 48 hours of incubation, RNA was collected from the cells for analysis.

Clinical Samples From Patients With MASLD/MASH

Surgically resected specimens from patients with MASLD/MASH were obtained with approval from the Institutional Review Board at Osaka University Hospital (IRB No. 15267).

RNA-seq of Patient Liver Biopsy Samples

We previously reported and published the results of liver tissue RNA-seq from 98 patients with NAFLD/nonalcoholic steatohepatitis (NASH) (GSE167523).[20] Based on the clinical data, we confirmed that NAFLD corresponds to non-MASH and that NASH corresponds to MASH, and we reanalyzed the raw count data using iDEP_2.01.

Spatial Transcriptome Analysis

Formalin-fixed paraffin-embedded (FFPE) liver tissue sections from patients with MASH-related HCC were cut at a 5-μm thickness and mounted onto CosMx-compatible slides. Samples were prepared according to the manufacturer's protocol (NanoString Technologies). Anti-B2M/CD298, anti-PanCK, anti-CD45, and anti-CD3 antibodies, together with 4′,6-diamidino-2-phenylindole (DAPI), were used as morphological markers. Gene expression was profiled using the CosMx Human Universal Cell Characterization RNA Panel (1000-plex).

Cell segmentation was performed for all cells within the available fields of view (FOVs) on a single slide containing

both tumor and non-tumor regions. Preliminary analysis, cell typing, and microenvironment (niche) annotations were conducted using the AtoMx Spatial Informatics Platform (NanoString). Cell type assignments were guided by the Human Liver RDS reference from the CellProfileLibrary and were manually curated. Transcript coordinate visualization and cell type/niche rendering were performed within AtoMx, and resulting images were exported.

Cell metadata, expression matrices, transcript coordinates, FOV coordinates, cell type annotations, and niche classifications were exported as a Seurat object for downstream analysis in R. For this study, analyses were restricted to non-tumor regions. Pairwise intercellular distances were computed from XY coordinate data using the Euclidean distance, and the minimum distance between specified cell type pairs was extracted.

We comprehensively assessed LR interactions by extracting 364 one-to-one LR pairs from the CellChat database present within the 1000-plex panel. Spatial LR scores were computed by integrating LR expression levels with directional spatial proximity between cell types. Interactions between identical cell types (self-self pairs) were excluded to focus on intercellular rather than autocrine signaling.

All computational workflows, including Seurat processing, cell type annotations, directional spatial proximity scoring, and spatial LR weighting, are openly available on Zenodo together with the Seurat objects, metadata, and expression matrices (https://doi.org/10.5281/zenodo.14921039 for data; https://doi.org/10.5281/zenodo.17532914 for the analysis code and documentation), ensuring full reproducibility.

Statistical Analyses

Statistical analyses were performed using GraphPad Prism 10.1.1 (GraphPad Software). For analyses not specifically mentioned, the following statistical tests were used:

For comparisons between 2 groups in in vitro experiments, assuming normality, an unpaired Student's *t*-test was used. For comparisons involving 3 or more groups, 1-way analysis of variance (ANOVA) was followed by Tukey's post hoc test for multiple comparisons. When each group was compared with the control group, Dunnett's multiple comparisons test was applied. For comparisons involving multiple groups with 2 factors, such as the presence or absence of LPS and PA, 2-way ANOVA was performed, followed by Šídák's multiple comparisons test. For in vivo studies, normality was first assessed using the Shapiro-Wilk test for all data. If normality was confirmed, the same statistical tests used for the in vitro experiments, such as Student's *t*-test and 1-way ANOVA, were applied. If normality was not confirmed, nonparametric tests were used, with the Mann-Whitney *U* test used for comparisons between 2 groups. All bar plots in the figures are presented as the means ± standard errors of the mean (SEM) unless otherwise noted.

Supplementary Material

Note: To access the supplementary material accompanying this article, visit the full text version at https://doi.org/10.1016/j.jcmgh.2025.101698.

References

1. Allen AM, Younossi ZM, Diehl AM, et al. Envisioning how to advance the MASH field. Nat Rev Gastroenterol Hepatol 2024;21:726–738.
2. **Targher G**, **Byrne CD**, **Tilg H**. MASLD: a systemic metabolic disorder with cardiovascular and malignant complications. Gut 2024;73:691–702.
3. Loomba R, Friedman SL, Shulman GI. Mechanisms and disease consequences of nonalcoholic fatty liver disease. Cell 2021;184:2537–2564.
4. Kolodziejczyk AA, Zheng D, Shibolet O, et al. The role of the microbiome in NAFLD and NASH. EMBO Mol Med 2019;11:e9302.
5. Tincopa MA, Anstee QM, Loomba R. New and emerging treatments for metabolic dysfunction-associated steatohepatitis. Cell Metab 2024;36:912–926.
6. Swanson KV, Deng M, Ting JP. The NLRP3 inflammasome: molecular activation and regulation to therapeutics. Nat Rev Immunol 2019;19:477–489.
7. Petrasek J, Bala S, Csak T, et al. IL-1 receptor antagonist ameliorates inflammasome-dependent alcoholic steatohepatitis in mice. J Clin Invest 2012;122:3476–3489.
8. Negash AA, Ramos HJ, Crochet N, et al. IL-1β production through the NLRP3 inflammasome by hepatic macrophages links hepatitis C virus infection with liver inflammation and disease. PLoS Pathog 2013;9:e1003330.
9. **Kong X**, **Liu W**, Zhang X, et al. HIF-1α inhibition in macrophages preserves acute liver failure by reducing IL-1β production. FASEB J 2023;37:e23140.
10. An L, Wirth U, Koch D, et al. The role of gut-derived lipopolysaccharides and the intestinal barrier in fatty liver diseases. J Gastrointest Surg 2022;26:671–683.
11. Tripathi A, Debelius J, Brenner DA, et al. The gut-liver axis and the intersection with the microbiome. Nat Rev Gastroenterol Hepatol 2018;15:397–411.
12. Csak T, Ganz M, Pespisa J, et al. Fatty acid and endotoxin activate inflammasomes in mouse hepatocytes that release danger signals to stimulate immune cells. Hepatology 2011;54:133–144.
13. **Wen H**, **Gris D**, Lei Y, et al. Fatty acid-induced NLRP3-ASC inflammasome activation interferes with insulin signaling. Nat Immunol 2011;12:408–415.
14. MacParland SA, Liu JC, Ma XZ, et al. Single cell RNA sequencing of human liver reveals distinct intrahepatic macrophage populations. Nat Commun 2018;9:4383.
15. Xiong X, Kuang H, Ansari S, et al. Landscape of intercellular crosstalk in healthy and NASH liver revealed by single-cell secretome gene analysis. Mol Cell 2019;75:644–660.e5.
16. Tanaka S, Hikita H, Tatsumi T, et al. Rubicon inhibits autophagy and accelerates hepatocyte apoptosis and lipid accumulation in nonalcoholic fatty liver disease in mice. Hepatology 2016;64:1994–2014.
17. Zhong Z, Umemura A, Sanchez-Lopez E, et al. NF-κB restricts inflammasome activation via elimination of damaged mitochondria. Cell 2016;164:896–910.
18. Settembre C, Di Malta C, Polito VA, et al. TFEB links autophagy to lysosomal biogenesis. Science 2011;332:1429–1433.

19. **Nakamura S**, **Shigeyama S**, **Minami S**, et al. LC3 lipidation is essential for TFEB activation during the lysosomal damage response to kidney injury. Nat Cell Biol 2020;22:1252–1263.
20. Kozumi K, Kodama T, Murai H, et al. Transcriptomics identify thrombospondin-2 as a biomarker for NASH and advanced liver fibrosis. Hepatology 2021;74:2452–2466.
21. **Gracia-Sancho J**, **Caparrós E**, **Fernández-Iglesias A**, et al. Role of liver sinusoidal endothelial cells in liver diseases. Nat Rev Gastroenterol Hepatol 2021;18:411–431.
22. McConnell MJ, Kostallari E, Ibrahim SH, et al. The evolving role of liver sinusoidal endothelial cells in liver health and disease. Hepatology 2023;78:649–669.
23. Gehrke N, Hofmann LJ, Straub BK, et al. Hepatic interleukin-1 receptor type 1 signalling regulates insulin sensitivity in the early phases of nonalcoholic fatty liver disease. Clin Transl Med 2022;12:e1048.
24. Ćurčić IB, Kizivat T, Petrović A, et al. Therapeutic perspectives of IL1 family members in liver diseases: an update. J Clin Transl Hepatol 2022;10:1186–1193.
25. Mirea AM, Tack CJ, Chavakis T, et al. IL-1 family cytokine pathways underlying NAFLD: towards new treatment strategies. Trends Mol Med 2018;24:458–471.
26. Dasarathy S, Mitchell MC, Barton B, et al. Design and rationale of a multicenter defeat alcoholic steatohepatitis trial: (DASH) randomized clinical trial to treat alcohol-associated hepatitis. Contemp Clin Trials 2020;96:106094.
27. **Larsen CM**, **Faulenbach M**, **Vaag A**, et al. Interleukin-1-receptor antagonist in type 2 diabetes mellitus. N Engl J Med 2007;356:1517–1526.
28. van Asseldonk EJ, van Poppel PC, Ballak DB, et al. One week treatment with the IL-1 receptor antagonist anakinra leads to a sustained improvement in insulin sensitivity in insulin resistant patients with type 1 diabetes mellitus. Clin Immunol 2015;160:155–162.
29. Chao X, Wang S, Zhao K, et al. Impaired TFEB-mediated lysosome biogenesis and autophagy promote chronic ethanol-induced liver injury and steatosis in mice. Gastroenterology 2018;155:865–879.e12.
30. Kim SH, Kim G, Han DH, et al. Ezetimibe ameliorates steatohepatitis via AMP activated protein kinase-TFEB-mediated activation of autophagy and NLRP3 inflammasome inhibition. Autophagy 2017;13:1767–1781.
31. Song JX, Sun YR, Peluso I, et al. A novel curcumin analog binds to and activates TFEB in vitro and in vivo independent of MTOR inhibition. Autophagy 2016;12:1372–1389.
32. **Zhang J**, **Wang J**, Xu J, et al. Curcumin targets the TFEB-lysosome pathway for induction of autophagy. Oncotarget 2016;7:75659–75671.
33. Komatsu M, Waguri S, Ueno T, et al. Impairment of starvation-induced and constitutive autophagy in Atg7-deficient mice. J Cell Biol 2005;169:425–434.
34. Okabe K, Kobayashi S, Yamada T, et al. Neurons limit angiogenesis by titrating VEGF in retina. Cell 2014;159:584–596.
35. Kodama T, Takehara T, Hikita H, et al. Increases in p53 expression induce CTGF synthesis by mouse and human hepatocytes and result in liver fibrosis in mice. J Clin Invest 2011;121:3343–3356.
36. Liu J, Huang X, Werner M, et al. Advanced method for isolation of mouse hepatocytes, liver sinusoidal endothelial cells, and kupffer cells. Methods Mol Biol 2017;1540:249–258.
37. Chanput W, Mes JJ, Wichers HJ. THP-1 cell line: an in vitro cell model for immune modulation approach. Int Immunopharmacol 2014;23:37–45.
38. Saito Y, Hikita H, Nozaki Y, et al. DNase II activated by the mitochondrial apoptotic pathway regulates RIP1-dependent non-apoptotic hepatocyte death via the TLR9/IFN-β signaling pathway. Cell Death Differ 2019;26:470–486.
39. Sakane S, Hikita H, Shirai K, et al. White adipose tissue autophagy and adipose-liver crosstalk exacerbate nonalcoholic fatty liver disease in mice. Cell Mol Gastroenterol Hepatol 2021;12:1683–1699.

Author names in bold indicate shared co-first authorship.

Received March 12, 2025. Accepted November 26, 2025.

Correspondence
Address correspondence to: Tetsuo Takehara, MD, PhD, Department of Gastroenterology and Hepatology, The University of Osaka, Graduate School of Medicine, 2-2 Yamadaoka, Suita, Osaka 565-0871, Japan. e-mail: takehara@gh.med.osaka-u.ac.jp.

Acknowledgments
The authors thank Professor Masaaki Komatsu for providing the Atg7flox/flox mice.

CRediT Authorship Contributions

Kenji Fukumoto, MD (Conceptualization: Equal; Data curation: Lead; Formal analysis: Lead; Funding acquisition: Supporting; Investigation: Lead; Methodology: Lead; Project administration: Equal; Resources: Supporting; Validation: Lead; Visualization: Lead; Writing – original draft: Lead; Writing – review & editing: Supporting)

Hayato Hikita, MD, PhD (Conceptualization: Equal; Data curation: Supporting; Formal analysis: Supporting; Funding acquisition: Equal; Methodology: Supporting; Project administration: Equal; Resources: Equal; Supervision: Supporting; Validation: Supporting; Writing – original draft: Supporting; Writing – review & editing: Equal)

Yoshinobu Saito, MD, PhD (Data curation: Supporting; Formal analysis: Supporting; Methodology: Supporting; Supervision: Supporting; Validation: Supporting; Writing – original draft: Supporting; Writing – review & editing: Supporting)

Yuki Makino, MD, PhD (Data curation: Supporting; Formal analysis: Supporting; Methodology: Supporting)

Kazumasa Soma, MD (Data curation: Supporting; Methodology: Supporting)

Seiya Kato, MD (Data curation: Supporting; Resources: Supporting)

Yoichi Sasaki, MD (Data curation: Supporting; Resources: Supporting)

Yuta Myojin, MD, PhD (Data curation: Supporting)

Katsuhiko Sato, MD, PhD (Data curation: Supporting)

Sadatsugu Sakane, MD, PhD (Data curation: Supporting; Methodology: Supporting)

Kazuhiro Murai, MD, PhD (Data curation: Supporting; Methodology: Supporting)

Yuki Tahata, MD, PhD (Data curation: Supporting)

Takahiro Kodama, MD, PhD (Methodology: Supporting)

Tomohide Tatsumi, MD, PhD (Methodology: Supporting)

Daisuke Motooka, PhD (Formal analysis: Supporting; Software: Lead; Writing – review & editing: Supporting)

Yoshiaki Kubota, MD, PhD (Resources: Supporting; Writing – review & editing: Supporting)

Shogo Kobayashi, MD, PhD (Resources: Supporting; Writing – review & editing: Supporting)

Hidetoshi Eguchi, MD, PhD (Resources: Supporting; Writing – review & editing: Supporting)

Tetsuo Takehara, MD, PhD (Conceptualization: Lead; Data curation: Supporting; Funding acquisition: Equal; Methodology: Supporting; Project

administration: Equal; Supervision: Lead; Validation: Supporting; Writing – original draft: Supporting; Writing – review & editing: Equal)

Conflicts of interest
The authors disclose no conflicts.

Funding
This work was partly supported by the Japan Agency for Medical Research and Development (AMED) (JP25fk0210121 to Hayato Hikita and Tetsuo Takehara; JP25gm0010012 to Hayato Hikita) and by the Japan Society for the Promotion of Science (JSPS) (JP21H02903 to Tetsuo Takehara; JP23H02894 to Hayato Hikita).

Data Availability
The single-cell RNA sequencing data from the mouse liver have been deposited in the NCBI Gene Expression Omnibus (GEO) under accession number GSE291866. The Seurat objects, metadata, and expression matrices for liver samples from 2 patients with MASH analyzed using CosMx spatial transcriptomics are publicly available on Zenodo under DOI: 10.5281/zenodo.14921039 (version v1.0). The analysis scripts (R code), updated README documentation, and derivative spatial analysis outputs generated in this study are available at Zenodo under DOI: 10.5281/zenodo.17532914 (version v1.1). All data and code necessary to reproduce the analyses in this manuscript are openly accessible.